Designing and Constructing a High-Resolution Imaging Apparatus

by

Michael Peter Kinach

NSERC USRA PROJECT REPORT

Supervisor: Dr. Kirk Madison

THE UNIVERSITY OF BRITISH COLUMBIA

(Vancouver)

August 2015

Abstract

This report details the development process of a high-resolution imaging apparatus. This apparatus will be used in the Quantum Degenerate Gases Laboratory to study mixtures of ultracold Li and Rb. The imaging apparatus is designed to capture images with a spatial resolution of 1-2 μm. To achieve this end, an aluminum mount for the imaging optics was designed using SolidWorks CAD software. This mount was then manufactured and the high-performance imaging optics were added. The imaging capabilities of the system were tested and it is found that the imaging system successfully achieves a maximum spatial resolution of approximately 2 μm. Several complications arose when the imaging system was installed into the Li-Rb experiment. In particular, the addition of the apparatus caused a reduction in the number of atoms that were captured in the magneto-optical trap of the experiment. This report includes a thorough description of the efforts that were made to diagnose and eliminate each complication. Also detailed are future plans for the imaging system and possible changes that could be made to improve the apparatus.

Contents

List of Figures

Chapter 1

Introduction & Theory

Experiments with ultracold quantum gases have been of great interest to the Atomic, Molecular and Optical Physics community in recent years. These experiments explore fundamental topics in quantum mechanics and contribute to fields as diverse as quantum optics, high-energy astrophysics and condensed matter physics [1]. Imaging techniques are commonly used to probe these ultracold systems. High-resolution techniques are advantageous because they allow for the detection of features that only appear on smaller length scales. With single-atom resolution, for example, the particle-particle correlations that characterize the quantum gas can be measured. Single-atom resolution was achieved with the development of the 'quantum gas microscope' in 2009 [2]. Scanning electron microscopy has also been used to image single atoms with a spatial resolution of about 150 nm [3]. Although these two imaging methods are powerful, they are very expensive and technically challenging.

This report details the development of a high-resolution imaging system in the Quantum Degenerate Gases Lab at the University of British Columbia. The system is designed to have a resolution of at least 2 μm. The project largely builds on the B.Sc. thesis work of Kahan Dare [4]. In Dare's thesis, a preliminary design for the high-resolution imaging system is presented. Many of the original considerations from that preliminary design have carried over to the final design. While this report is intended to be comprehensive, the reader may benefit from the additional background that is provided in Dare's thesis. The major focus of this report is to provide a thorough and detailed description of the work accomplished where Dare's thesis leaves off.

1.1 The Imaging Equation

In its simplest form, an imaging system requires only a lens and a camera. If an object is placed in front of the lens, the lens will produce an image of the object.

The location of an image can be calculated from the imaging equation[1]. We can write the imaging equation as

$$\frac{1}{f} = \frac{1}{d_o} + \frac{1}{d_i} \tag{1.1}$$

where f is the focal length of the imaging lens, d_o is the object distance and d_i is the image

[1] This equation is also known as the thin lens equation.

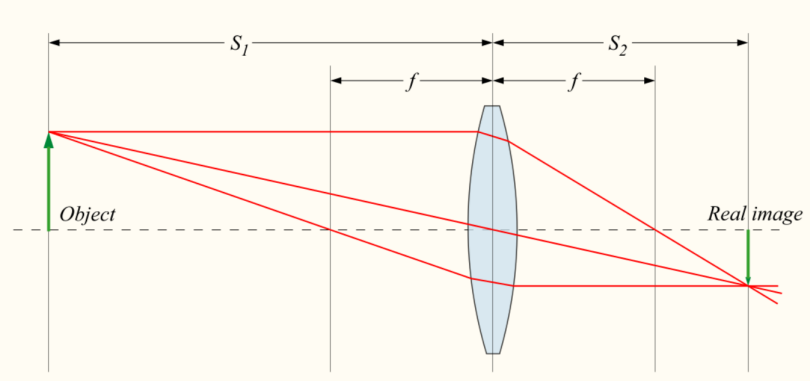

Figure 1.1: A diagram showing how an image is formed by a lens. An object is placed at a distance S_1 from the lens. The light rays coming from this object are refracted by the lens. The rays converge to form an image of the object at a distance S_2 from the lens. Image credit: https://commons.wikimedia.org/wiki/File:Lens3.png

distance. In Figure 1.1, S_1 is the object distance and S_2 is the image distance.

In our imaging system, the object is the cloud of ultracold particles. If the focal length of the lens is known and the object distance is specified then the image distance can be calculated. The image will be captured by a CCD camera in our system.

The imaging equation can also be used to determine the magnification of the imaging system. The optical magnification M of an object is the ratio between its apparent size and its true size. Mathematically, this ratio is equivalent to the ratio between d_i and d_o. We can use the fact that $M = \frac{d_i}{d_o}$ to rearrange Equation 1.1 and show that

$$\frac{d_o}{f} = \frac{1}{M} + 1. \tag{1.2}$$

One can see that $M \to \infty$ as $d_o \to f$. This means that the object should be placed at a distance that is close to the focal length of the imaging lens to achieve a large magnification.

1.2 Optical Aberration

Small misalignments and flaws in the imaging optics can reduce the quality of the final image. There are also some types of aberration that are inherent in any imaging system. It is important to minimize these aberrations so that a high-resolution can be achieved.

1.2.1 Spherical Aberration

Spherical aberration occurs when the light rays that pass through a lens do not meet at a single focal point. Instead, the light that strikes the lens near its edge refracts to a greater degree than the light that strikes near the center.

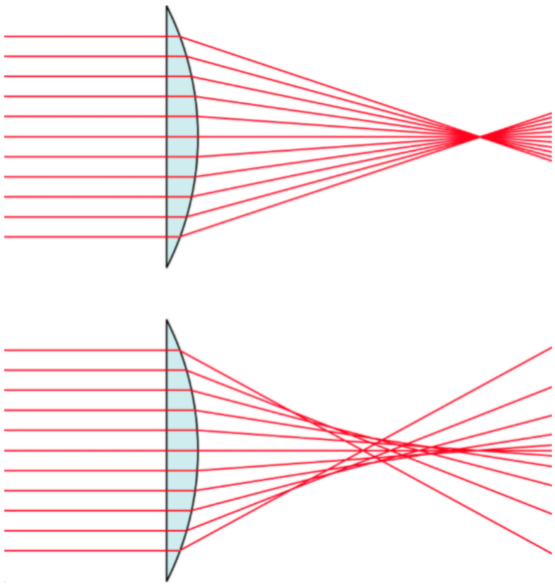

Figure 1.2: An illustration of spherical aberration. In the top image, the light rays are uniformly refracted by the lens so that the beam reaches a focus at a single point. In the bottom image, the rays do not converge to a single point. This is known as spherical aberration. Chromatic aberration is similar in that light of different wavelengths is focused at different distances.

1.2.2 Chromatic Aberration

Chromatic aberration occurs when different wavelengths of light converge at different locations. This is similar to spherical aberration except that the focal location of the rays depends only on the wavelength. This type of aberration is not very important for our imaging system because the images will be captured using only 671 nm light.

1.2.3 Coma and Astigmatism

Optical coma occurs when light passes through the lens at an angle or off-center. This results in the image having a comet-like tail. Astigmatism occurs when light rays propagating in perpendicular planes converge to different focal points. When astigmatism is present, the image may be blurred or defocused in one direction.

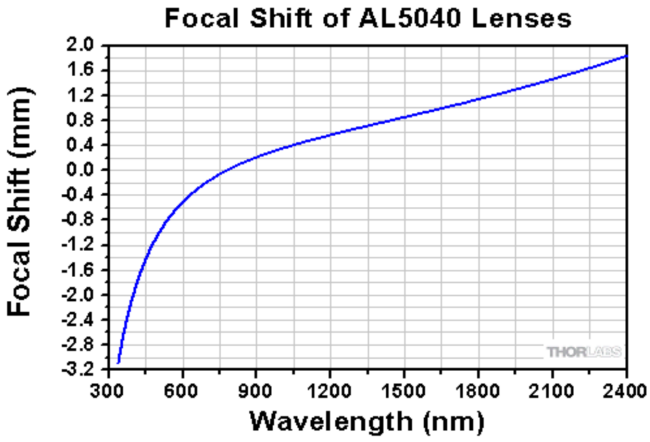

Figure 1.3: A graph of chromatic aberration data for the ThorLabs Al5040-B lens. The design wavelength of the lens is 780 nm (focal shift of 0 mm). Image credit: http://www.thorlabs.com/thorproduct.cfm?partnumber=AL5040-B

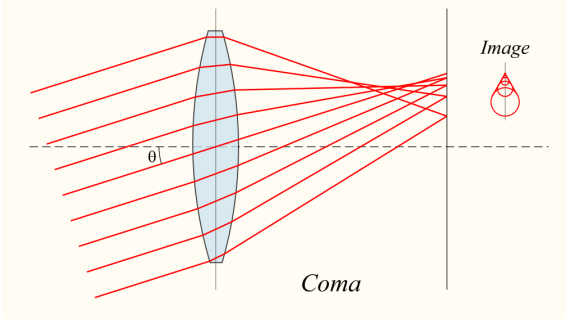

Figure 1.4: An illustration of coma aberration. The light rays pass through the lens at an angle. This results in the image having a comet-like tail. Image credit: https://en.wikipedia.org/wiki/Coma_%28optics%29#/media/File:Lens-coma.svg

Chapter 2

Imaging System Design

The first step in building a high-performance optical system is a carefully-designed computer model. To this end, a 3D model was created in SolidWorks, a computer-aided design (CAD) program. The CAD drawings of the design were then given to the machine shop for construction.

In this report, the machined components of the imaging system will be referred to as the as the 'imaging mount'. The term 'imaging system' will refer to the machined components with all of the imaging optics attached.

2.1 Considerations for the Imaging System

There are many factors that have to be considered when designing an imaging system. For example, the system must be compatible with the other features of the experiment. The system must also be made as compact as possible so that it can fit into the experimental setup and leave room for future additions.

2.1.1 Multiple Functions of the System

Absorption Imaging

This system is designed to satisfy several important functions. Its primary purpose is to capture high-resolution absorption images of ultracold particles in an optical lattice. This requires two main components: an imaging lens and a camera. It is important that these two components are placed at an appropriate distance away from each other so that images of the particles can be captured.

Magneto-Optical Trap

The system is also responsible for handling the vertical arm of the magneto-optical trap (MOT). The vertical arm of the MOT consists of two vertical, counter-propagating laser beams. These beams must be collimated and circularly-polarized with the correct 'handedness'. The imaging system must be able to hold the optics for the vertical arm of the MOT.

Vertical Lattice

The third function of the imaging system is to generate a vertical lattice potential that can spatially confine the ultracold particles. The imaging system must hold the optics for this lattice.

2.1.2 Selection of Imaging Optics

The final design of the imaging system was largely dictated by the choice of imaging optics. The selected optic for imaging was a ThorLabs AL5040-B 50mm aspheric lens. The lab purchased this lens several years ago with imaging applications in mind. This aspheric lens is shaped to reduce chromatic and spherical aberrations. This is the same lens that was used in Dare's thesis and was shown to achieve a resolution of at least 2 μm [4].

The lab also possessed a ThorLabs DMLP900L 2" dichroic mirror. This dichroic mirror transmits 1064 nm light and reflects 671-780 nm light. The MOT beam and the beam used for imaging the particles are both at 671 nm while the vertical lattice beam is at 1064 nm. The dichroic mirror makes it possible to separate these two wavelengths. This optic was also purchased in advance of the work described in this report.

2.1.3 Physical Constraints of the Experimental Setup

The imaging system is designed to capture images from underneath the vacuum cell. However, there are two magnetic field coil mounts that take up most of the space above and below the cell. The lower coil imposes a significant physical constraint on the imaging system. The vacuum cell and magnetic field coils are depicted in Figure 2.1.

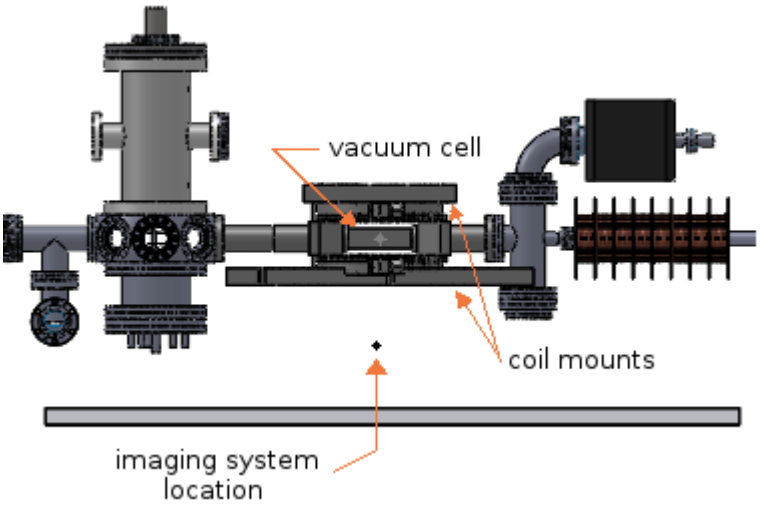

Figure 2.1: A model of the experimental setup. The location of the vacuum cell and the magnetic field coil mounts are highlighted. The imaging system is placed under the lower coil mount.

Fortunately, the coil mounts were designed with a large central hole. This hole is centered on the cell and has a diameter of 60 mm. The imaging lens can be easily placed within this hole because it has a diameter of 50 mm.

In order to appreciate the constraint imposed by the coil mount, it is first necessary to consider the height at which the lens will be placed in the hole. For high-resolution imaging, it is often favourable to have a large magnification so that neighbouring particles can be easily differentiated. According to the imaging equation (Equation 1.1), the magnification of a system depends on the distance between the lens and the object being imaged. In our experiment, the target object is the cloud of particles in the cell. Since the height of the lens inside the hole will determine how far it is from the cell, the overall magnification of the imaging system depends on this height.

Unfortunately, the imaging lens cannot be placed very high in this hole because it has a short focal length. This short focal length causes the MOT beam, which passes through the center of the imaging lens, to quickly converge and then quickly diverge. If the imaging lens is placed too high then the MOT beam will be clipped by the additional optics in the imaging system[2]. This scenario is illustrated in Figure 2.2.

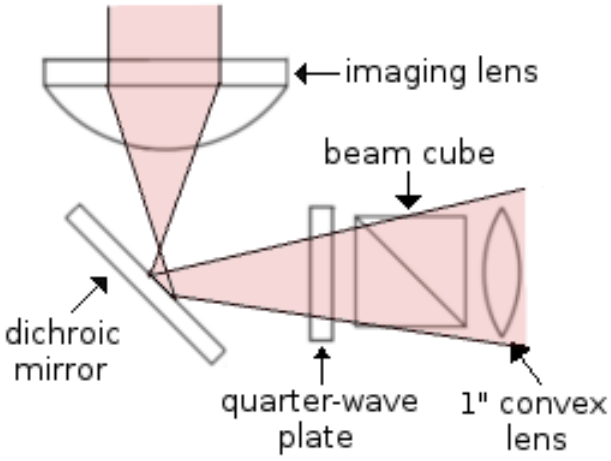

Figure 2.2: A sketch illustrating a clipping MOT beam. The red MOT beam is focused by the imaging lens and bounces off of the dichroic mirror. Notice how this diverging beam does not fit into the 1" convex lens. If the lens is placed too high, the amount of light that is clipped on this lens will increase. If the MOT beam is clipped, the quality of the magneto-optical trap will suffer.

The imaging mount is also designed to take advantage of a small cutout in the bottom of the coil mounts. This cutout allows for the imaging system to be placed at a slightly greater height then would otherwise be possible. The extra height slightly reduces the clipping of the MOT beam.

[2]Due to the limited space in the coil hole, these additional optics can only be placed underneath the coil mount.

2.2 Design of an Aluminum Mount

An imaging mount was designed to accommodate the optics for all three functions of the imaging system. The physical constraints of the experiment were considered during the design process.

The aluminum imaging mount is composed of four separate pieces that can be fastened together. These four components are named 'top', 'vertical', 'sidemount' and 'horizontal'. The CAD drawings for these parts can be found in the appendix to this report.

Top Component

The constraints of the coil mount hole and the large size of the imaging lens makes it difficult to hold the lens inside the hole using traditional mounts. The primary purpose of the top component is to hold the imaging lens.

The lens is supported from below by a long, thin cylindrical neck. This neck fits inside the coil mount hole so that the lens can be placed close to the vacuum cell. Since the coil mount hole has a diameter of 60 mm, the neck has an outer diameter of 58 mm. This difference of 2 mm ensures that the lens can be easily raised and lowered within the hole. More information about mounting the lens can be found in Subsection 2.3.1.

The 'top' component is also milled out on one side so that a ThorLabs H45CN 45° dichroic mirror mount can be fastened to it.

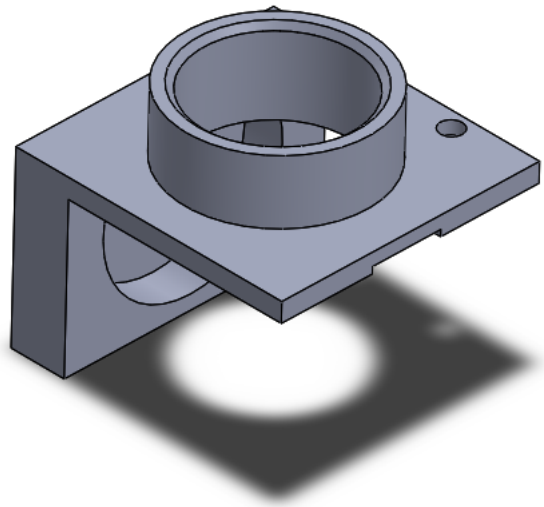

Figure 2.3: The 'top' component of the imaging mount. The metal cylinder on the top holds the imaging lens.

Vertical Component

The 'vertical' component acts as the body of the imaging mount. It anchors the other three components of the mount and can be attached to a Newport 562-XYZ three-dimensional translation stage. Like the 'top' component, the 'vertical' component is milled out on its front face so that a ThorLabs H45CN 45° dichroic mirror mount can be fastened to it. This mirror mount will eventually hold the optic that reflects the vertical lattice beam.

Sidemount Component

This is an arm that holds the optics for separating the MOT beam and the imaging beam. It is screwed onto the front face of the 'vertical' component. The 'sidemount' has two unthreaded holes on either side of a central platform. These holes allow for a quarter-wave plate and a 1" lens to be mounted using ThorLabs LMR1 1" mounts. The central platform is designed to hold a polarizing beam cube that reflects light downwards. This requires that the platform has a central hole through which the light can pass. The hole size was maximized so that as much light as possible can pass through the platform.

Since the 'sidemount' component is designed to be as close to the dichroic mirror as possible, one corner of the 'sidemount' is chamfered. This ensures that the 'sidemount' does not collide with the 45° dichroic mirror mount attached to the 'top' component. Note also that a small portion of the 'top' component was milled so that the wave plate mount could fit properly.

Horizontal Component

The 'horizontal' component attaches to the 'vertical' component. It can be screwed to the translation stage which provides greater stability for the entire imaging mount. Threaded holes were also added to both the 'vertical' component and the 'horizontal' component so that a triangular brace can add additional stability.

2.3 Arrangement of Imaging Optics

The most important consideration for an imaging system is how its optical components will be arranged and aligned. Even a slight misalignment can cause aberrations that reduce the image quality. Small deviations can also reduce the effectiveness of the MOT and vertical lattice. It is therefore necessary to carefully plan the arrangement and alignment of optics in the imaging system.

2.3.1 Mounting the Imaging Lens

The lens is supported by the long, cylindrical neck on the 'top' component. This neck maximizes the usable area of the lens by only touching the lens at the edges. The inside edge of the neck

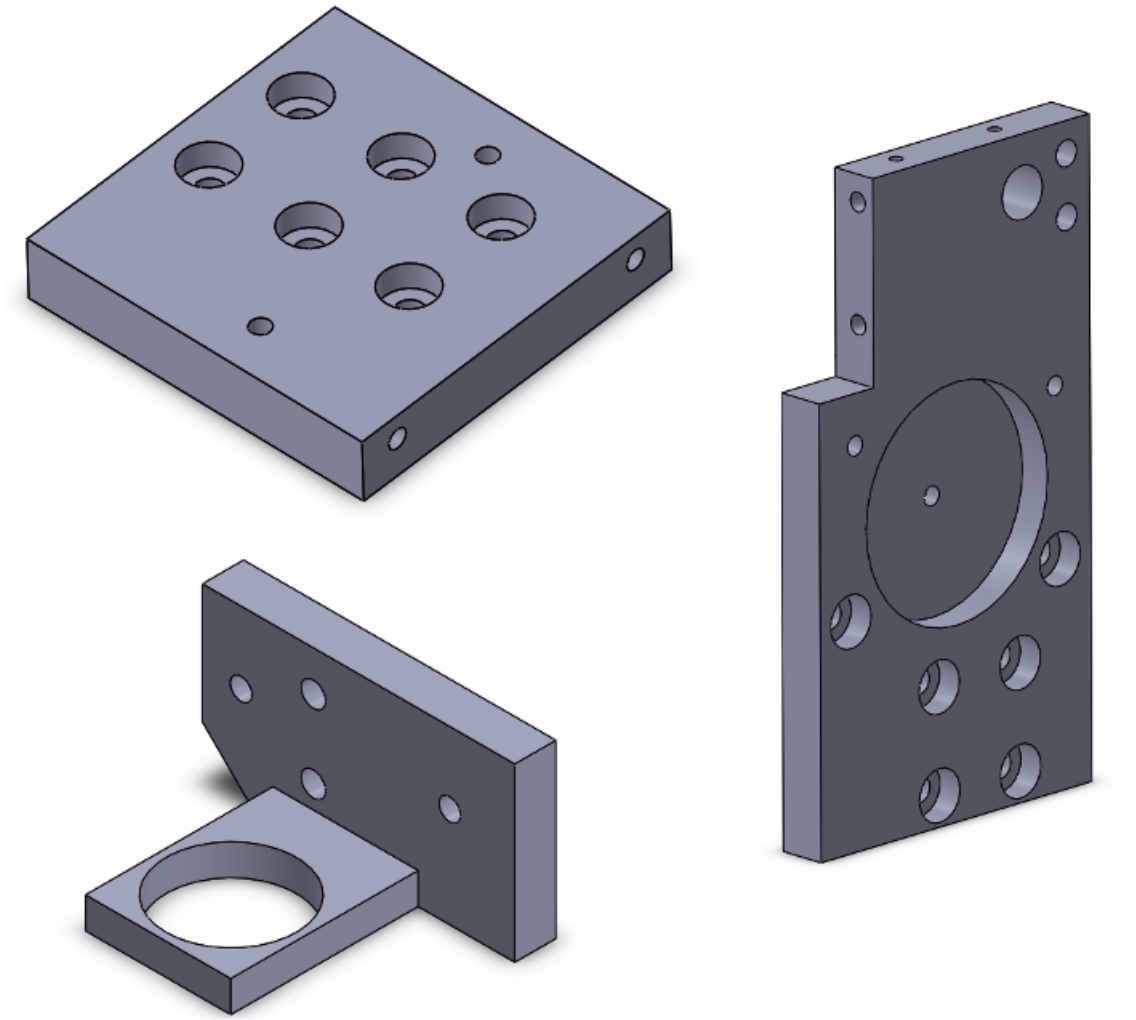

Figure 2.4: Clockwise from top left: the 'horizontal', 'vertical' and 'sidemount' components of the imaging mount. The central platform in the 'sidemount' component holds the beam cube. The 'horizontal' component can be attached to the 'vertical' component and the translation stage to add stability to the system.

was chamfered to ensure a snug fit for the lens. This chamfer aligns with the contours of the lens so that the lens can be easily placed on the top of the neck. This chamfer also prevents the lens from being damaged by the sharp inner edge of the neck.

The height of the neck was chosen based on our selection of a magnification factor of 25 times. This factor was chosen because it minimizes the clipping of the MOT beam while still providing an adequate magnification for high-resolution imaging. When the lens is in place, there is approximately 43 mm between the cell and the lens. It is important to note that the reference focal location of the imaging lens is not the flat face. Instead, it is inset from the flat face of the lens by approximately 5 mm. This information comes from the specifications of the lens provided on the ThorLabs website[3].

The lens was glued. Care was taken to make sure that the lens was flat and centered on the mount before it was permanently secured.

The centering of the imaging lens was straightforward. Since the chamfer aligns with the contours of the lens, it was quite easy to place the lens in the center of the cylinder. The outer diameter of the cylinder is only 2 mm smaller than the coil mount hole. This means that the imaging system can be placed within this hole with only a few millimeters of room for horizontal translation.

Details about gluing the lens are provided in Subsection 3.1.2.

2.3.2 Placement of the Dichroic Mirror

A 2" dichroic mirror was placed below the lens to separate the MOT beam and imaging beam from the vertical lattice beam. The dichroic mirror was mounted in a 45° ThorLabs H45CN mount. The final design allows for the 671 nm beams to be reflected horizontally and the 1064 nm beam to be transmitted vertically through the mirror. The dichroic mirror was placed as close to the imaging lens as possible. This is because the short focal length of the lens causes the MOT beam to come to a focus and diverge very rapidly (Figure 2.2).

The transmitted light passes through the hole in the back of the dichroic mount. Unfortunately, this hole is not centered on the dichroic mirror. That is, a beam passing through the centre of the 45° dichroic mirror will not pass through the center of the hole[4]. For this project, it was reasoned that the priority goes to centering the MOT beam and imaging beam on the mirror. This is because the imaging functionality and MOT functionality of the imaging system are vital to its performance but the vertical lattice is not[5].

When the dichroic mirror is placed in the H45CN mount it becomes clear that there is some wasted space at the front of the mount. The final design reduces this wasted space by milling the

[3] http://www.thorlabs.com/thorproduct.cfm?partnumber=AL5040-B

[4] The center of the dichroic mirror was taken to be the center of the top face.

[5] In retrospect, it probably would have been wiser to center the hole for the vertical lattice light. After all, the MOT beam and imaging beam will both be converging when they hit the dichroic mirror. It is unlikely that they would have clipped on the dichroic mirror.

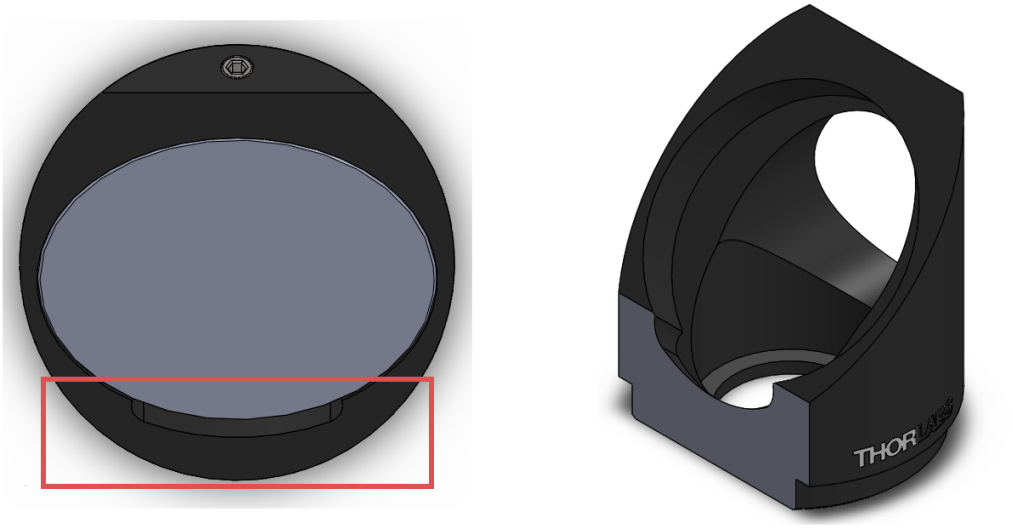

(a) (b)

Figure 2.5: (a) A top-down view of the ThorLabs H45CN dichroic mirror mount with the dichroic mirror in place. The red box highlights the portion of the mount that was cut to save space in the imaging system. (b) A model of the dichroic mirror mount after modification.

front of the mount. This reduces the distance between the imaging lens and the dichroic mirror. Milling the front of the mount has the added benefit of reducing the rotational freedom of the mirror.

To further reduce the distance between the lens and the mirror, an acrylic spacer was laser cut to raise the height of the dichroic mirror in the mount. Without the acrylic spacer, the mirror would lie 4 millimeters lower in the mount. The spacer raises the face of the mirror so that it is in line with the flat face of the mount.

The transmitted 1064 nm light hits a second mirror that lies below the dichroic mirror. This second mirror is mounted in a 45° H45CN mount. It is fastened to the 'vertical' component of the imaging system. It reflects the 1064 nm light in a different direction than the above dichroic mirror.

2.3.3 Separating the MOT and Imaging Beams

After passing through the lens, the 671 nm beams are reflected horizontally by the dichroic mirror. These beams pass through the optics mounted on the 'sidemount' component.

The first component is a quarter-wave plate. Both the imaging beam and the MOT beam need to be circularly polarized when they pass through the cell. This wave plate changes the polarization of both beams from circular to linear.

The beams then pass through a polarizing beam cube. The cube is oriented so that any

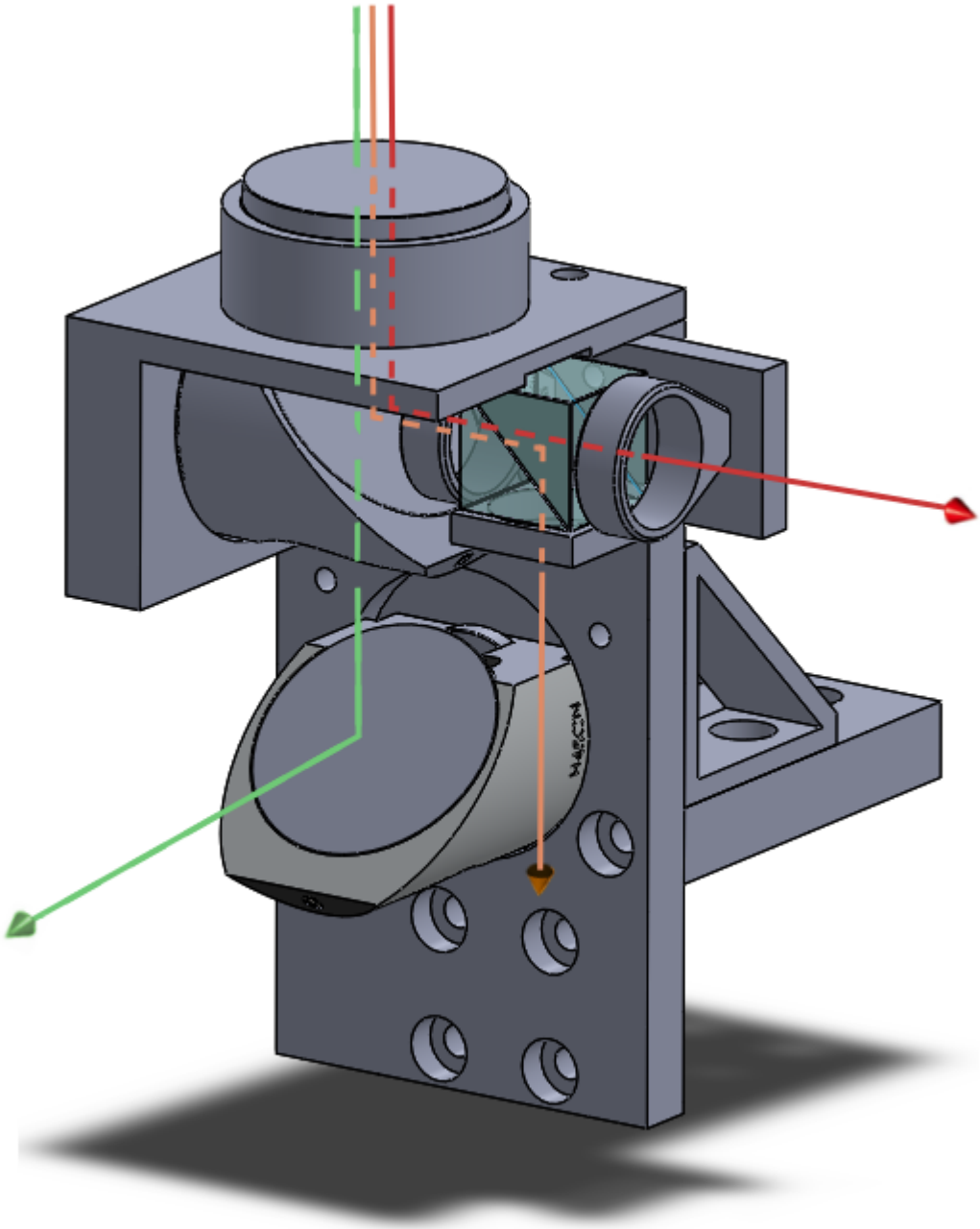

Figure 2.6: A SolidWorks model of the assembled imaging system showing the beam paths. The red line shows the path of the 671 nm MOT beam through the imaging system. The orange line shows the path of the 671 nm imaging beam. The green line shows the path of the 1064 nm vertical lattice beam. The dichroic mirror separates the 671 nm beams from the 1064 nm beam. The polarizing beam cube separates the MOT beam and imaging beam.

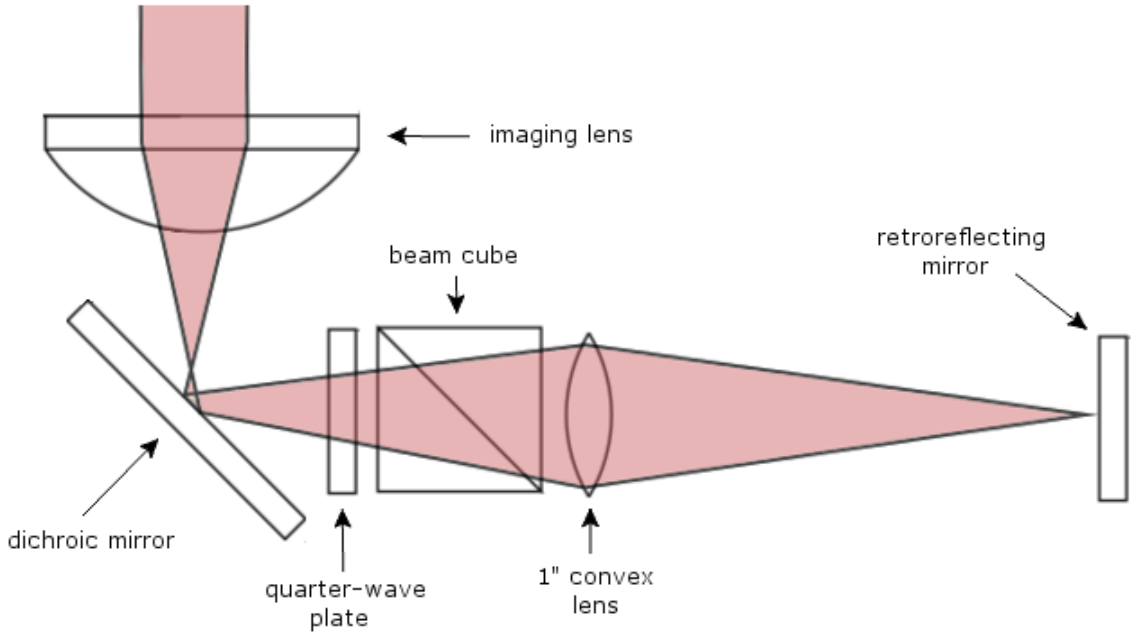

Figure 2.7: A sketch of how the MOT beam propagates through the imaging system. After passing through the 1" convex lens, the beam begins to converge. A plane mirror is placed at the focus of this converging beam to send it back through the imaging system. In contrast to Figure 2.2, the MOT beam is not clipped in this sketch.

horizontally polarized light is reflected downwards and any vertically polarized light transmits straight through the cube. In our setup, the imaging light is reflected and the MOT light is transmitted. Both beams need to have a specific initial polarization so that they can be fully reflected or transmitted by the beam cube. Otherwise, the MOT quality and image quality will be reduced.

After transmitting through the beam cube, the MOT beam encounters a 1" convex lens. The MOT beam is diverging at this point[6]. The optical components were positioned as close to the dichroic mirror as possible to reduce the clipping of the MOT beam. This 1" lens counteracts the divergence of the MOT beam and causes the beam to converge. A plane mirror can be placed at the focus of this converging beam. The beam is retroreflected at this mirror and passes backwards through the 1" lens, beam cube and wave plate. It is then recollimated by the imaging lens and overlaps with the incoming MOT beam to form the z-arm of the magneto-optical trap.

The imaging light is reflected by the cube and travels downwards towards the optical table. A mirror can be placed here to redirect the imaging light into the camera.

[6]The MOT beam comes to a focus very near to the surface of the dichroic mirror (roughly 40mm from the reference focal location of the lens). It starts diverging from there.

2.4 Capturing Images

The primary function of the imaging system is to capture high-resolution images of particles in the vacuum cell. According to the imaging equation (Equation 1.1), the distance at which an image is formed depends on both the focal length of the lens and the distance between the lens and the object. The imaging equation shows that the image magnification depends on how close the lens is placed to the object.

The imaging lens in this setup has a focal length of 40 mm. The object being imaged is the cloud of particles in the cell. The magnification of the imaging system was chosen to be 25 times. With these parameters it is straightforward to determine that placement of the CCD camera should be 1040 mm away from the lens.

As explained in the previous section, the imaging light will bounce down from the beam cube. This light can be redirected by a 45° mirror and sent horizontally along the optical table.

2.4.1 Focusing the Image

Focusing an image at a high magnification can be quite challenging. Equation 1.1 implies that the image distance climbs rapidly as the object distance approaches the focal length of the lens. This means that it becomes difficult to focus an image at high magnifications because small deviations in image distance will put the image out of focus.

Since it is much easier to focus an image at low magnifications, the strategy is to first locate a focused image of the object at 1-3 times magnification and then slowly increase it. To increase the magnification one must iteratively raise the height of the lens and move the camera backwards[7]. For example:

- adjust the height of the lens so that an image can be formed with a magnification of 1-3 times
- adjust the camera until an image is formed on the CCD sensor
- when the image is in focus, adjust the lens height by translating it toward the object (the image becomes slightly defocused but still visible)
- move the camera backwards to compensate; the image comes back into focus and appears slightly larger
- repeat until an appropriate magnification is achieved

The height of the lens can easily be adjusted because the imaging mount is on a three-dimensional translation stage. To facilitate the translation of the camera across the breadboard,

[7]Although we did not get the chance to capture image of atoms in the dipole trap during the course of this project, this method was successfully used to locate the image of a pinhole at 25 times magnification.

a temporary track was used. The track is composed of several 80-20 metal posts that are secured to the breadboard. A simple mount for the camera is built so that the camera can slide along the posts with only one degree of freedom.

2.4.2 CCD Camera

The CCD camera being used is a Point Grey FL2G-13S2M-C. This camera has a pixel resolution of 1288 x 964 and a maximum frame rate of 30 FPS. The pixel size is 3.75 μm. The FLEA2 camera operates via a FireWire 1394b connection. This camera was only found to work with a Texas Instruments FireWire card. Several other cards were tried, such as a VIA FireWire card and a NEC FireWire card, but neither was compatible with the FLEA2.

Chapter 3

Alignment and Testing

3.1 Adding the Imaging Optics

Most of the optics were relatively straightforward to fasten to the imaging mount. The wave plate, dichroic mirror and 1" lens could easily be screwed in. The beam cube and imaging lens, on the other hand, both had to be glued.

3.1.1 Gluing the Beam Cube

An acrylic alignment tool was laser cut so that the beam cube could be easily centered on its platform. There were two options for glue: a viscous 5-minute epoxy and a thin, watery Krazy Glue. The Krazy Glue was chosen because the thickness of the 5-minute epoxy could have affected the flatness of the cube. The glue was added to the four corners of the platform and the cube was then placed using the alignment tool.

3.1.2 Gluing the Lens

There was some discussion as to how flat we really needed the lens to be. If the lens was not sufficiently flat when glued, the beams that transmit through the lens would have passed through at an angle. This could have resulted in a coma or astigmatism that reduces the maximum resolution of the imaging system. It could have also caused aberrations in the vertical lattice beam and the MOT beam.

If we only wanted to reduce the possibility of astigmatism then we did not have to be very precise; a slightly angled lens probably wouldn't have significantly affected the image quality. However, since we were concerned with implementing a vertical lattice, we had to be make sure that we could image the atoms in the lattice effectively. A slight angle in the lens would also add a slight angle the vertical lattice 'pancake potentials'. This slight angle could have a disastrous effect for imaging because it would prevent us from fully imaging a single 'pancake'.

It was decided that imaging these 'pancake potentials' was not a big concern. The field of view of our imaging system is large enough that we are still able to image a 'pancake' even if the potentials are slightly angled.

To ensure that the lens was flat, a piece of acrylic was laser cut the held the lens in place. The acrylic piece had three points of contact with the edges of the lens. The acrylic piece also

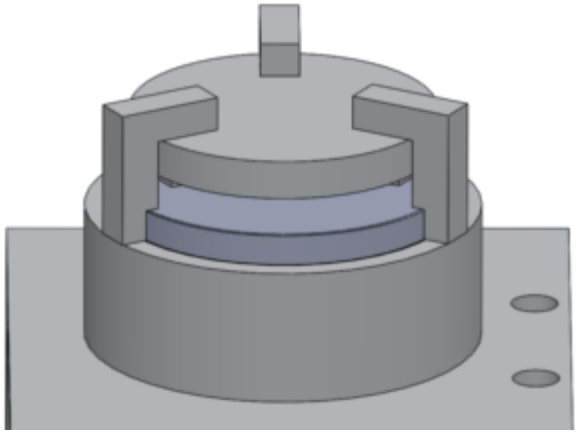

Figure 3.1: A SolidWorks model of the acrylic tool used to align the imaging lens. The three arms of the tool pressed down on the edges of the lens.

touched the aluminum neck. This design ensured that the height of the flat face of the lens above the neck was equal at three points. It was decided that this precision would meet our criteria for flatness.

The lens was then glued in place with 5-minute epoxy. The lens alignment piece was left on the lens while the glue dried to prevent the lens from shifting position. The glue was only applied at three places around the lens so that, if need be, the lens could still be removed.

3.2 Testing the System

The imaging system was tested outside the ultracold molecule experiment before it was installed. The main function of the testing phase was to (a) provide a rough idea for the order of magnitude of the resolution and (b) provide some practice for setting up the imaging system.

3.2.1 Setup

A 1 μm pinhole was used to characterize the system. This pinhole was illuminated using 780 nm light.

The lens was placed below the pinhole at some object distance d_o. The light from the pinhole propagated through the imaging system as shown in Figure 2.6. The FLEA2 camera was placed at an appropriate image distance to record the image.

After the pinhole was located at a low magnification, the magnification was increased until it was approximately 25 times. This was checked by measuring the image distance with a meter stick and a caliper.

The magnification was also verified by translating the pinhole. If the pinhole is translated across the object plane then one will observe a corresponding translation of the image across

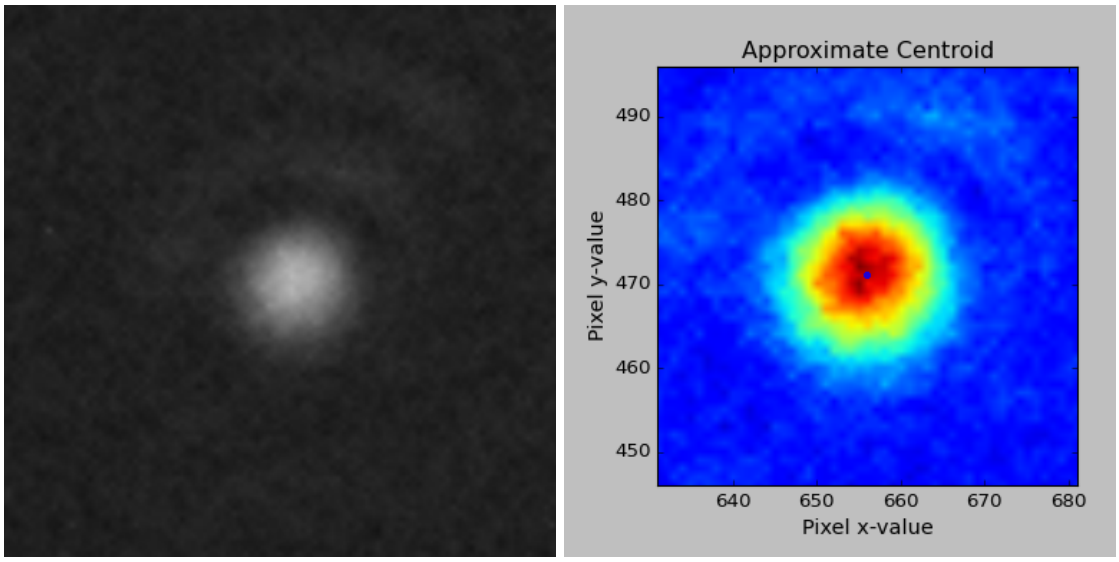

(a) (b)

Figure 3.2: (a) A picture of a pinhole at approximately 25 times magnification. (b) The same pinhole as in (a) with its calculated centroid given by the blue dot. The Python script calculated the FWHM based on the centroid position.

the image plane. By first taking a picture of the pinhole, translating it some known distance, and taking another picture, one can infer the magnification by comparing the two images and by using the pixel size of the CCD camera. The ratio between how far the pinhole appeared to be translated on the camera and how far it was actually translated will give the magnification. This was done using the Python script included in the appendix.

Once the magnification was verified as approximately 25 times, the position of the lens was adjusted to get rid of any obvious astigmatisms.

3.2.2 Determining the Resolution

After the magnification was determined, the pinhole images were analyzed to estimate the maximum resolution of the imaging system. A Python script was written to take a pinhole image, locate its centroid and output the full-width at half maximum (FWHM) along two axes. This FWHM was compared to the magnification and the size of the pinhole (1 μm) to provide an estimate for the resolution. The code for this script is included in the appendix.

It should be noted that the calculations presented here are not meant to be rigorous. A rigorous analysis had already been done in the B.Sc. thesis work of Kahan Dare [4]. Moreover, characterization work is planned for when the imaging system is fully installed in the experiment. For these reasons, it made sense to skip a rigorous analysis of the pinhole images in favour of using that time on the characterization work later in the project.

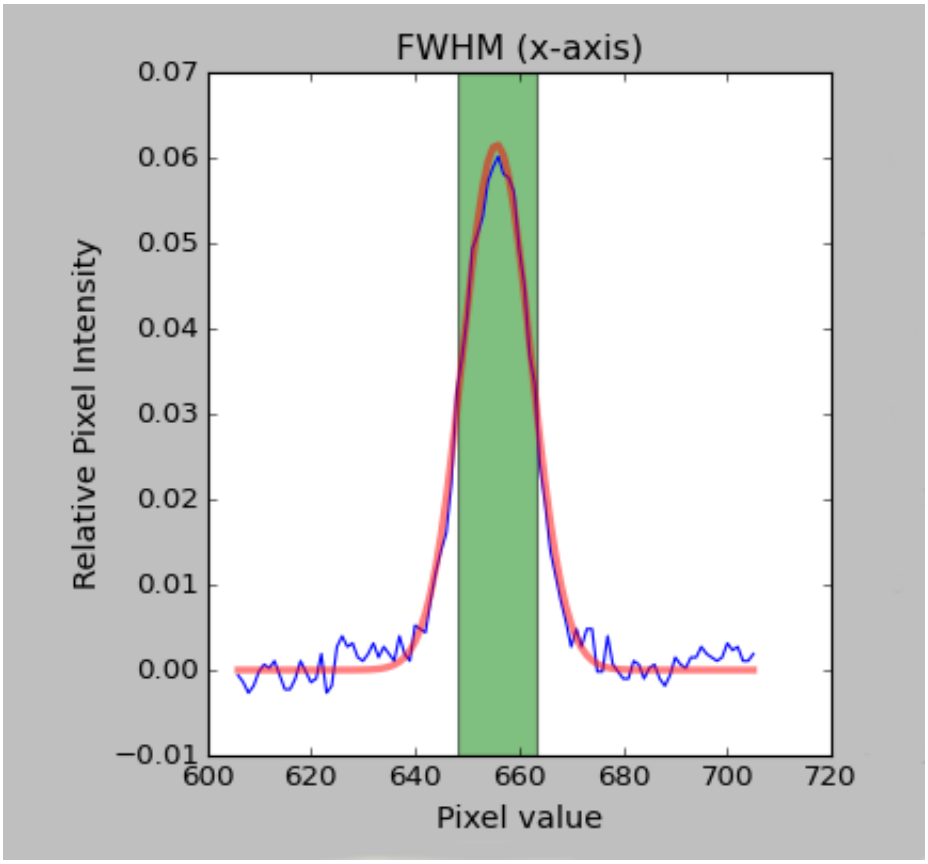

Figure 3.3: A graph of the FWHM along the x-axis for a pinhole image at approximately 25x magnification. The blue curve shows the actual pixel values from the image. The red curve shows an approximate Gaussian fit to the pixel data. The green shaded region highlights the part of the graph that is within the FWHM of the Gaussian fit.

The method used to estimate the spatial resolution during testing was to analyze the FWHM of the pinhole images. The pixel size of the camera is 3.75 μm. This value can be multiplied by the FWHM pixel value to get the FWHM in micrometers. Assuming that the 1 μm pinhole is a point source, and since the magnification is 25 times, this FWHM can be divided by 25 to get an estimate of the resolution capabilities of the system.

Now taking a quick estimate of the maximum resolution: the average FWHM for a sample of pinhole images was found to be approximately 15.2 pixels. Taking the pixel size and magnification into account, this corresponds to a spatial resolution of 2.28 μm. At first glance, this is somewhat alarming because it is above the expected resolution of 1-2 μm. However, there are several factors that may have inflated this number.

The first factor is that the magnification of 25 times was not exact. Although a caliper and a Python script were used to check the magnification, there is still uncertainty in this measurement. An off-the-cuff estimate based on several trials with the Python magnification program is ± 1

times.

The second factor is the use of 780 nm light. The Rayleigh criterion gives the spatial resolution as

$$\Delta l = 1.220\frac{\lambda f}{D} \tag{3.1}$$

where f is the focal length of the lens, λ is the wavelength of light being used, and D is the diameter of the lens' aperture. The spatial resolution is proportional to the wavelength of light being used. This means that we can expect the resolution for 780 nm light to be $\frac{780}{671} = 1.162$ times as large as that for 671 nm light. If this factor is taken into account, the resolution estimate drops from 2.28 μm to 1.96 μm for 671 nm light.

Due to both of these factors, the estimate for resolution was taken to be approximately 2 μm. In any case, the final characterization work will provide a better estimate of the system's capabilities.

Chapter 4

Installation

After testing was completed, the imaging system was installed in the ultracold molecule experiment. Several complications arose during this process. The imaging system had to be slightly modified to accommodate each complication.

4.1 The Presence of the Compensation Coils

When the imaging system was added to the experiment it did not fully insert into the coil mount hole. This was because the system was hitting the compensation coils that lie below the magnetic field coil mount. The compensation coils were not included in the SolidWorks drawing of the experimental setup and so were not accounted for in the design of the imaging system.

The presence of these coils pushed down the imaging system by approximately 9 mm. This increased the object distance of the imaging system to approximately 50 mm. This also reduced the maximum magnification. With a 50 mm object distance the maximum possible magnification was approximately 4 times.

There was no easy way to modify the compensation coils to sidestep this complication. It was possible to rebuild the compensation coils but this solution would have required a large amount of time. A second option was to buy a new imaging lens with a larger focal length. This would have allowed for a higher magnification without redesigning the entire system. Moreover, it would have significantly reduced the clipping of the MOT beam. The major downside to this option was the high cost of a new aspheric imaging lens. A quick search suggests that a new imaging lens would cost upwards of $500.

The simplest solution to make up for the loss in magnification was to use a secondary telescope after the imaging system. The magnification could then be increased without making any major changes to the system. The downside to this method is that the two additional lenses in the telescope could reduce the resolution by introducing additional aberrations.

4.2 The Effect of the Imaging System on the Magneto-Optical Trap

The first step in capturing images of ultracold particles is to get a MOT up and running. The MOT serves as the first stage in confining the ultracold particles. After the MOT, the particles are

further compressed and cooled before being loaded into the dipole trap. If the MOT is misshapen or there are a low number of atoms in the MOT then the dipole trap may not load. This makes it important for the MOT produced by the imaging system to be of a high quality.

The original setup for the magneto-optical trap is depicted in Figure 4.1. This is the setup before the imaging system was put into place. This setup was disassembled to make room for the imaging system.

With the imaging system in place, the MOT beam originated above the cell. It passed through the imaging system and was retroreflected at its focus. This setup is depicted in Figure 4.2.

4.2.1 Aberrations at the Focal Plane

There were clear aberrations in the MOT beam when it was sent through the imaging system. Near the plane of the final retroreflecting mirror, the MOT beam had a 'starburst' appearance. The severity of the 'starburst' increased as the propagation distance increased. The aberration remained even after several realignment attempts were made.

It is likely that these aberrations in the beam affected the quality of the MOT. The first MOT that was formed with the imaging system was very weak and misshapen. When the aberrated beam propagated back through the imaging system, the 1" 'sidemount' lens and the imaging lens likely distorted the beam further. This would have caused the two vertically-overlapping MOT beams to have radically different sizes and shapes. This effect probably caused the drop in MOT quality.

4.2.2 Reconstructing the Vertical Arm

A second setup for the vertical arm was introduced in an effort to increase the MOT quality. The setup had the MOT beam entering the system from below. As in the first setup, the beam was sent through a telescope to increase the size. The beam was bounced off of two 45° mirrors and sent through the 1" 'sidemount' lens. The beam came to a focus near the dichroic mirror where it bounced and started to diverge as it traveled upwards. This diverging beam was then collimated by the imaging lens. The beam was retroreflected above the cell.

One of the limitations of this setup was the fixed distance between the 1" 'sidemount' lens and the imaging lens. These lenses acted as a telescope that produced a collimated beam after the imaging lens. Since the position of these two lenses cannot be adjusted, the path length between them is fixed at 95 mm. In order to form a perfect telescope, these two lenses needed to have a combined focal length of 95 mm. This means that the focal length of the 1" lens had to be 55 mm because the imaging lens has a focal length of 40 mm.

Unfortunately, a $f = 55$ mm lens was not an optic that we had on hand. This means that the telescope could not be made perfect. Thus, the beam entering the 1" lens needed to be shaped so that a collimated beam could be produced by the imaging lens.

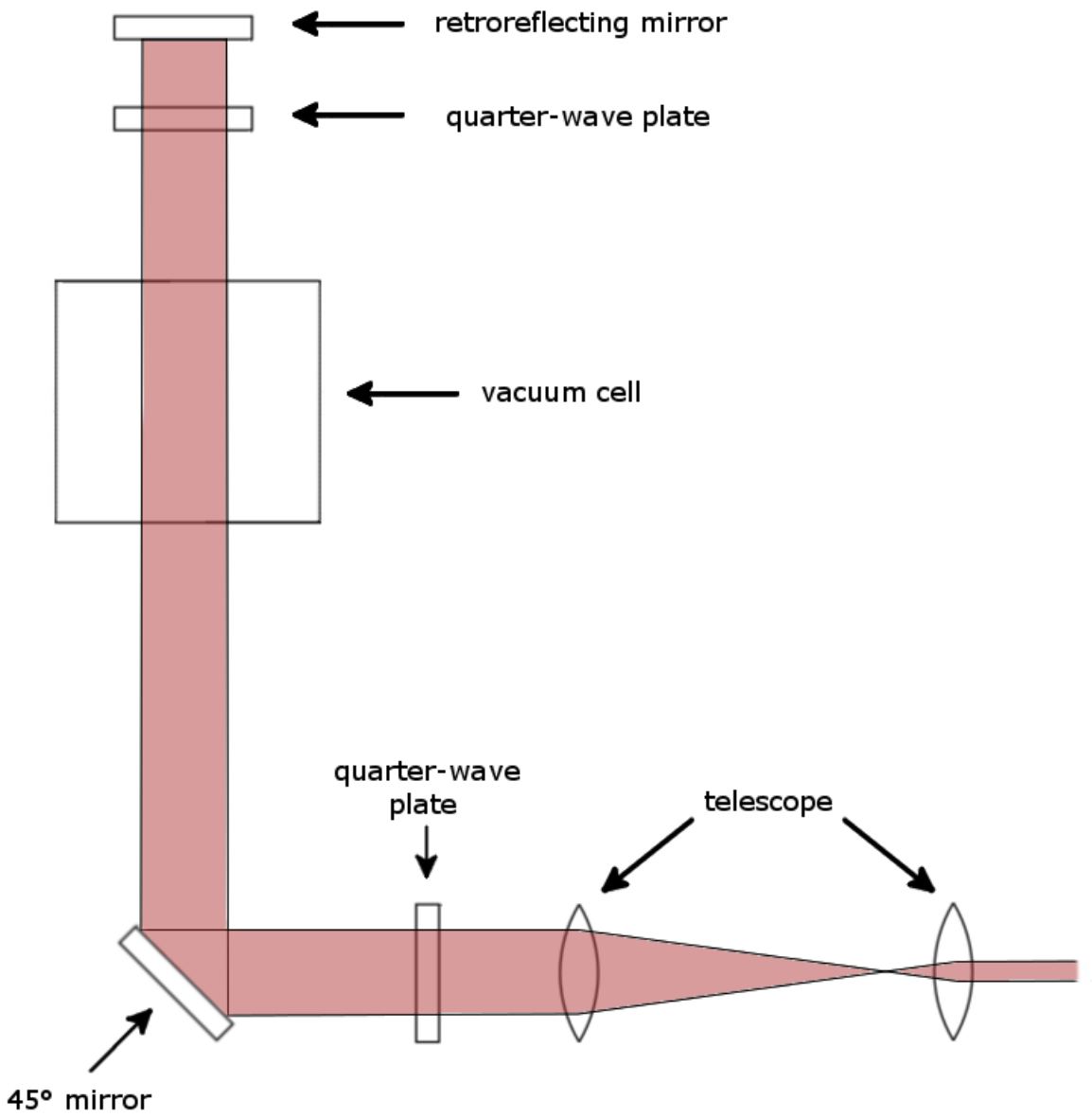

Figure 4.1: A simple sketch of the original setup for the vertical arm of the magneto-optical trap. The linearly-polarized beam is expanded by the telescope. It becomes circularly polarized after passing through the quarter-wave plate. It is then reflected up into the cell. The mirror and quarter-wave plate above the cell reflect the circularly-polarized beam (with the opposite 'handedness') back on itself.

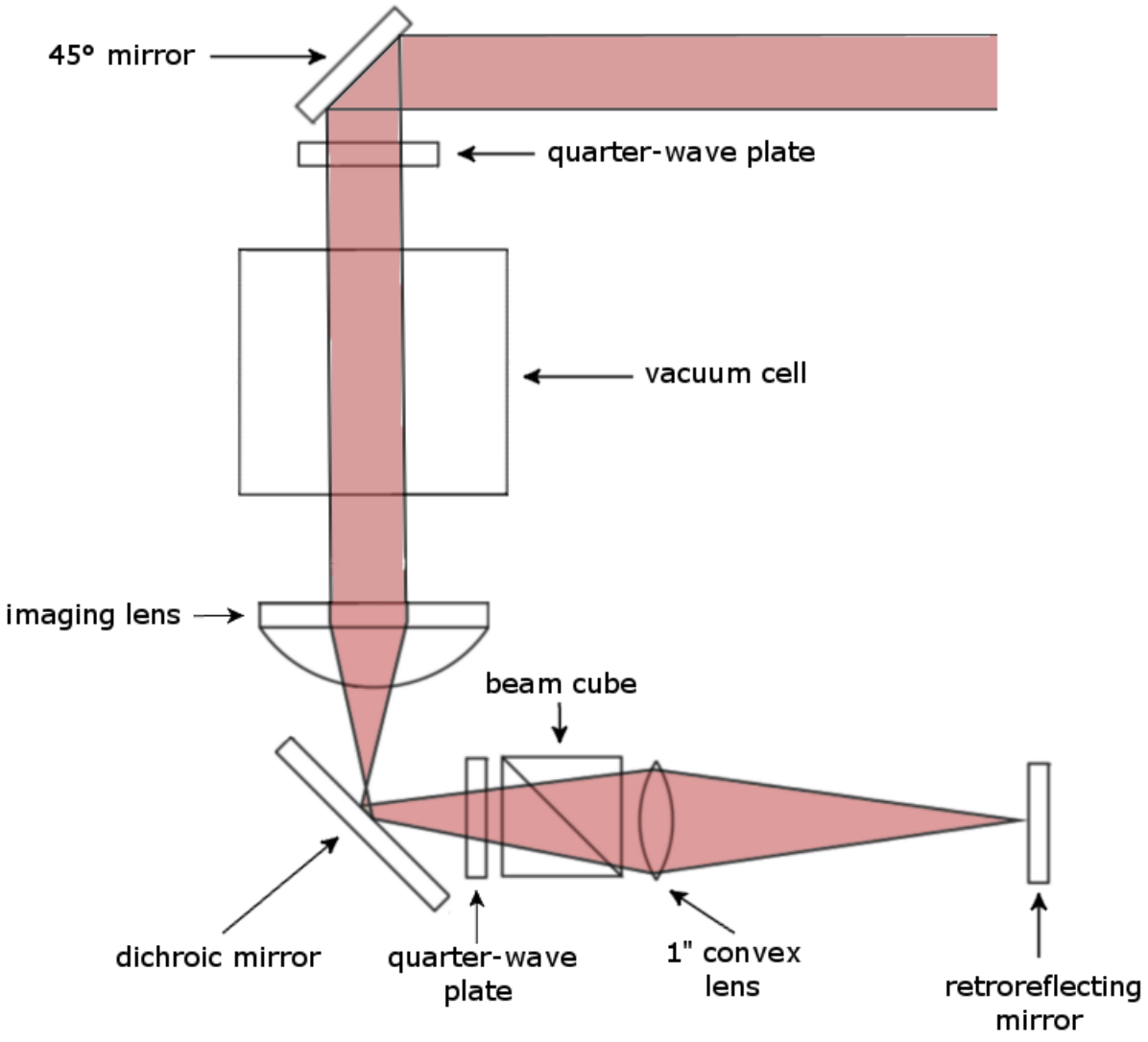

Figure 4.2: A simple sketch of the vertical arm of the MOT with the imaging system in place. The linearly-polarized beam is reflected off of a 45° mirror and sent through a quarter-wave plate. The light becomes circularly polarized and passes through the cell. It is focused by the imaging lens, reflected off of the 45° dichroic mirror and sent through a second quarter-wave plate. This beam transmits through the cube and is focused by a 1" lens. It is retroreflected at its focus and sent back through the imaging system.

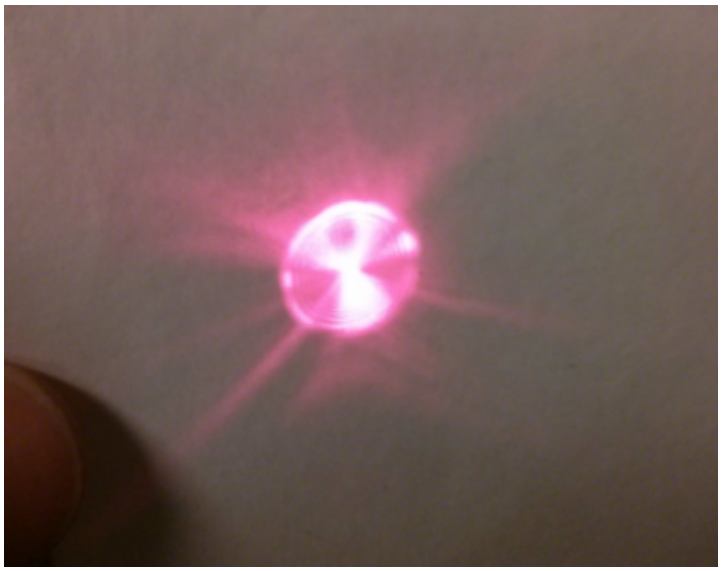

Figure 4.3: A picture of the MOT beam after it has passed through the imaging system. Note the clear aberrations that appear at the outer edges of the beam. These aberrations worsen as the beam propagates.

The closest lenses we had to a $f = 55$ mm lens were a $f = 40$ mm, a $f = 50$ mm and a $f = 75$ mm lens. These optics were all tried in place of the 1" 'sidemount' lens. The $f = 50$ mm lens was found to be the most suitable. The collimated beam that was produced when using the f =50 mm lens had a diameter of approximately 1 cm. Various other lens combinations were tried in an effort to increase the beam size. However, none of these changes had a significant impact on MOT quality.

4.2.3 The Appearance of MOT Beam Fringes

The collimated MOT beam in the second setup took on a 'bullseye' fringe pattern after being collimated by the imaging lens. This 'bullseye' pattern did not look Gaussian in shape and appeared to have interference-like fringes. One explanation for why the MOT beam did not look Gaussian is that the beam was getting clipped on one of the mirrors or lenses in the setup. The source of the fringe pattern was never conclusively determined.

Although the MOT beam appeared to be nicely collimated, the MOT still looked distorted. It did not look spherical and did not look very strong. If the Zeeman slower beam was blocked, the MOT drastically changed position or disappeared entirely.

Figure 4.4: A picture of the MOT beam after it is collimated by the imaging lens. Note the 'bullseye' pattern. This effect seemed to be more distinct for large beam diameters.

4.3 Testing the Imaging System Optics

Since the source of the problem could not be determined, the imaging system was disassembled so that the individual optics could be tested.

We first started by testing the beam cube and wave plate. Circularly-polarized light was sent through the beam cube. A power meter was used to check the amount of light that was transmitted and reflected. As expected, the beam cube split this light 50/50. A quarter-wave plate was then added in front of the cube. This wave plate was rotated until the majority of the light was transmitted through the cube. The wave plate was then secured to the 'sidemount' in this orientation. This test ensured that the maximum amount of MOT light would transmit through the cube.

We then checked the imaging lens[8]. A collimated beam with a large diameter was passed through the lens to simulate the MOT beam. This beam was then checked at the focal plane and in the far field. There were no noticeable aberrations or fringe patterns at the focus or in the far field. The fact that the imaging lens produced good images during the testing phase of the experiment also suggested that it wasn't the problem.

It was only when the imaging lens was used in a telescope that the fringe pattern reappeared. It is interesting to note that the imaging lens forms a telescope with the 1" convex lens in the 'sidemount'. This could explain the fringe pattern in Figure 4.4.

[8]We used a copy of the imaging lens for this purpose. We did not unglue the lens from the imaging mount.

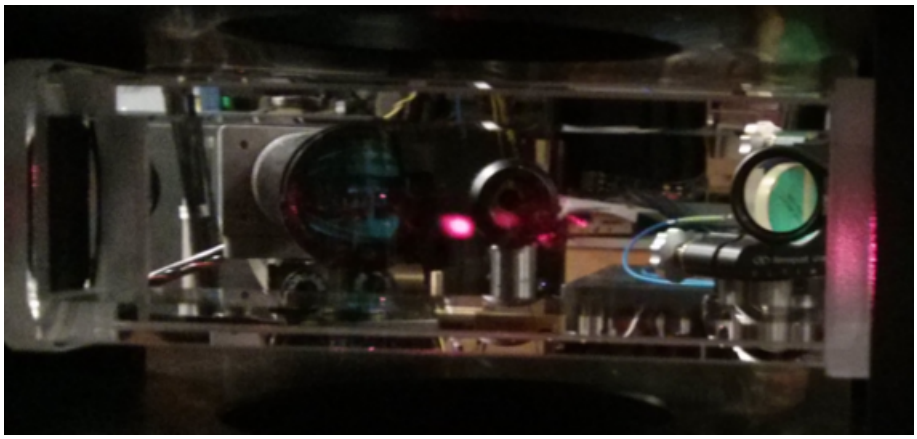

Figure 4.5: A picture of a strong MOT formed without the imaging system in place.

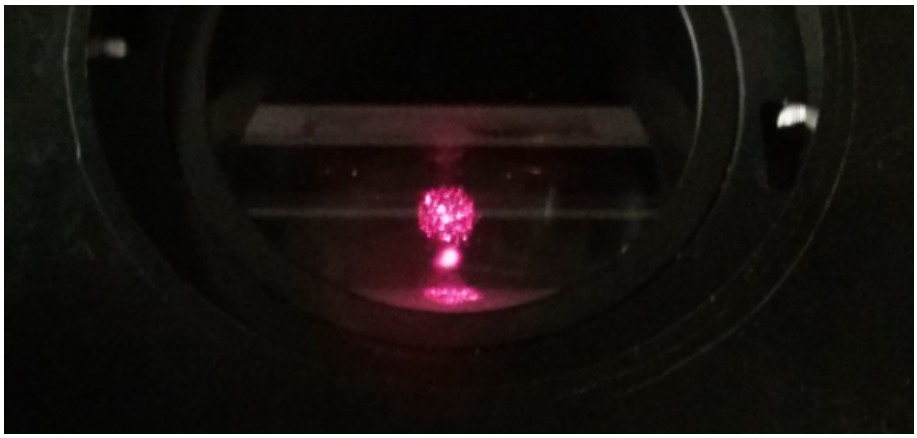

Figure 4.6: Another picture of the MOT, this time viewed from above. Note the size of the beam on the wall of the cell. This beam is approximately 1 cm in diameter.

4.4 The Effect of the Dichroic Mirror

The last optic to be tested was the dichroic mirror. We first reassembled the original MOT setup depicted in Figure 4.1. The dichroic mirror was added in place of the 45° plane mirror. This was found to drastically reduce the MOT quality. It was only after rotating the quarter-wave plate by approximately 45° that the MOT quality increased.

It appears that the birefringence of the dichroic mirror changed the polarization of the MOT beam. Instead of reflecting the circularly polarized light as expected, it was likely reflecting an elliptical polarization into the beam cube. This would reduce the amount of light that was transmitting through the cube. In effect, the dichroic mirror was acting like another wave plate in the imaging system. This also means that the beam traveling up through the cell may have been of some strange elliptical polarization that was detrimental to the MOT quality.

This complication was resolved by placing the quarter-wave directly below the cell. This change ensures that the MOT beam polarization is linear when it reflects off the dichroic mirror. If the quarter-wave plates are correctly aligned, the light that is incident on the dichroic mirror will be either entirely 'p'-polarized or entirely 's'-polarized. Since it would only be reflecting either 's' or 'p' linear light, the dichroic mirror cannot impose a phase change that will alter the polarization. This setup neutralizes the birefringent effects of the dichroic mirror and greatly improved the quality of the MOT. Visually, the MOT looked much stronger and much denser than with all previous attempts. A rough sketch of this new setup is depicted in Figure 4.7.

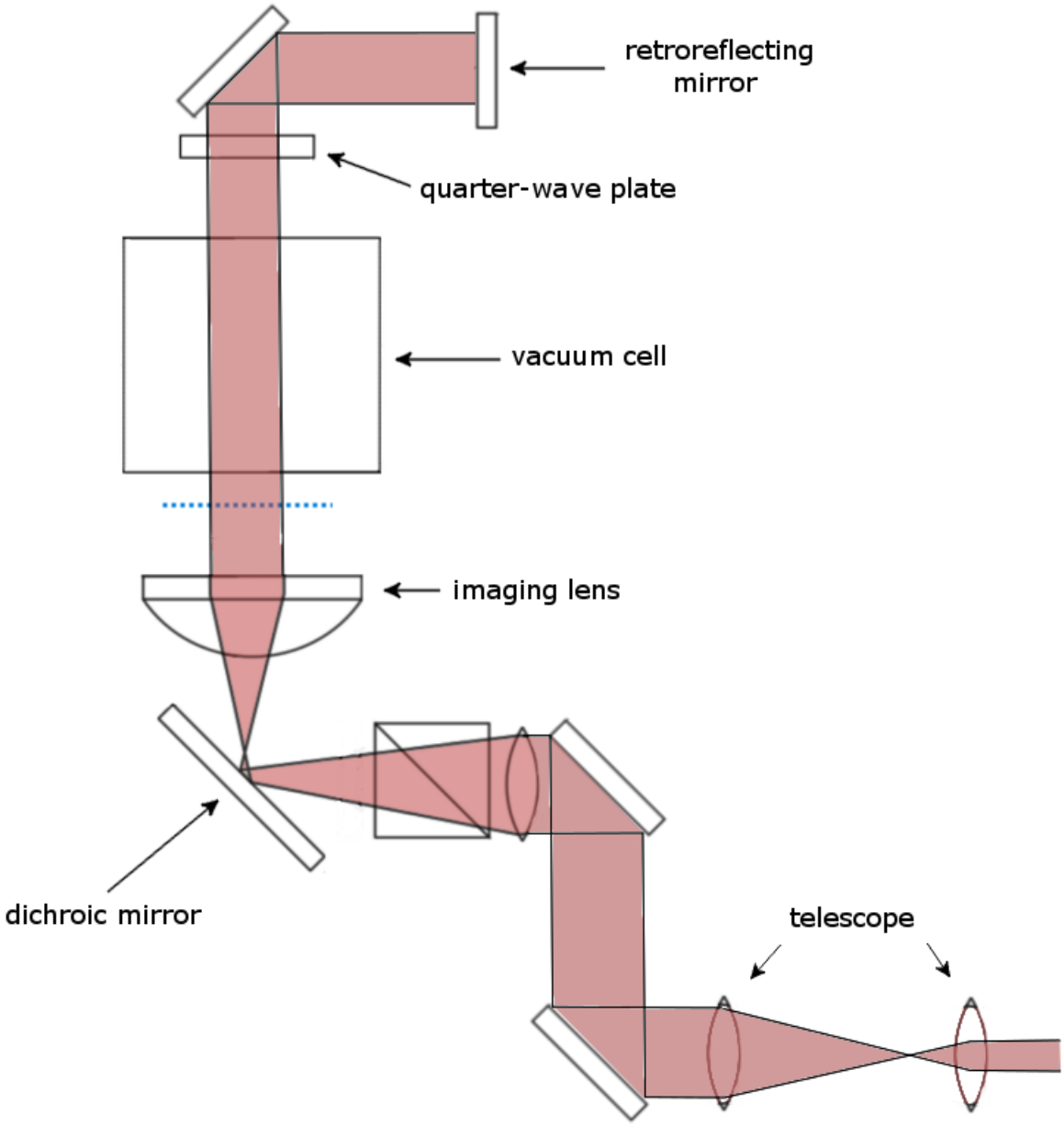

Figure 4.7: A sketch of the final setup for the vertical arm of the MOT. The beam originates from below the imaging system. The blue dotted line below the cell highlights the new location for the quarter-wave plate.

Chapter 5

Future Work and Recommendations

At the time of this writing, we have achieved a strong-looking MOT with the imaging system in place. Testing of the MOT will take place to ensure that the atom number is sufficient for loading the dipole trap. The dipole trap beams will be aligned and the vertical lattice will be implemented. A secondary telescope will also be added to make up for the loss of magnification. This will allow for characterization work to begin.

One way to characterize the imaging system is to image particles in an optical dipole trap. A dipole trap uses a high-power laser to provide an attractive potential to the particles held in a MOT. This attractive potential can spatially confine the atoms to 'pancake potentials' that can subsequently be imaged by the imaging system. These 'pancakes' will have spacings that are on the order of a micrometer and will therefore provide a good opportunity to test the capabilities of the imaging system.

A dilating lattice potential is another future project for the imaging system. Because it is often very difficult to detect and make measurements of single sites in an optical lattice, it would be advantageous to create a lattice that could be spatially tuned.[5] A dilating lattice would allow for this kind of dynamic control of the spacing between particles. Although more work still needs to be done before a dilating lattice can be implemented, it would be a great addition to the imaging system setup.

There are several changes that could be made to the imaging system to improve the overall design. For example, an imaging lens with a larger focal length could be used. This increase in focal length would compensate for the decrease in magnification caused by the presence of the compensation coils. A secondary telescope would no longer be needed and any reduction in resolution that would be caused by that additional telescope could be eliminated.

A lens with a higher focal length would also cause the MOT and imaging beam to diverge at a slower rate. The imaging optics in the system would not need to be so close together. Since one of the constraints of the system was how close the optics had to be squished together, this would open up the door for all sorts of redesign options.

Different optics could also be purchased to increase the performance of the system. If a dichroic mirror was acquired that did not have the drastic birefringent effects that we observed, we could mount the wave plate in its original position. A better mount for the dichroic mirror could also be machined or purchased so that the vertical lattice beam can transmit through the bottom of the mount with ease.

The main downside to these changes is that they carry heavy costs in both time and money. Many small changes could be made that would slightly improve the system but there is no single change that would drastically improve its performance. Buying a larger focal length lens, for example, would probably require an entirely new imaging mount to be designed and machined. This could take weeks or months of lab time to construct. This kind of drastic change would also probably require the imaging system to be retested and recharacterized.

As the imaging system is installed and characterized, it will become apparent if any changes are necessary.

Acknowledgments

First and foremost, I would like to thank my supervisor, Kirk Madison, for inviting me into his lab and allowing me to experience physics from a new perspective. I would also like to thank Kahan Dare for allowing me to pester him with questions day-in and day-out. I would not have learned nearly as much as I did without his help and guidance.

Finally, I would like to thank Will Gunton, Gene Polovy, Koko Yu, Kais Jooya and Janelle Van Dongen for their help and advice. I had a wonderful time working in the lab alongside them.

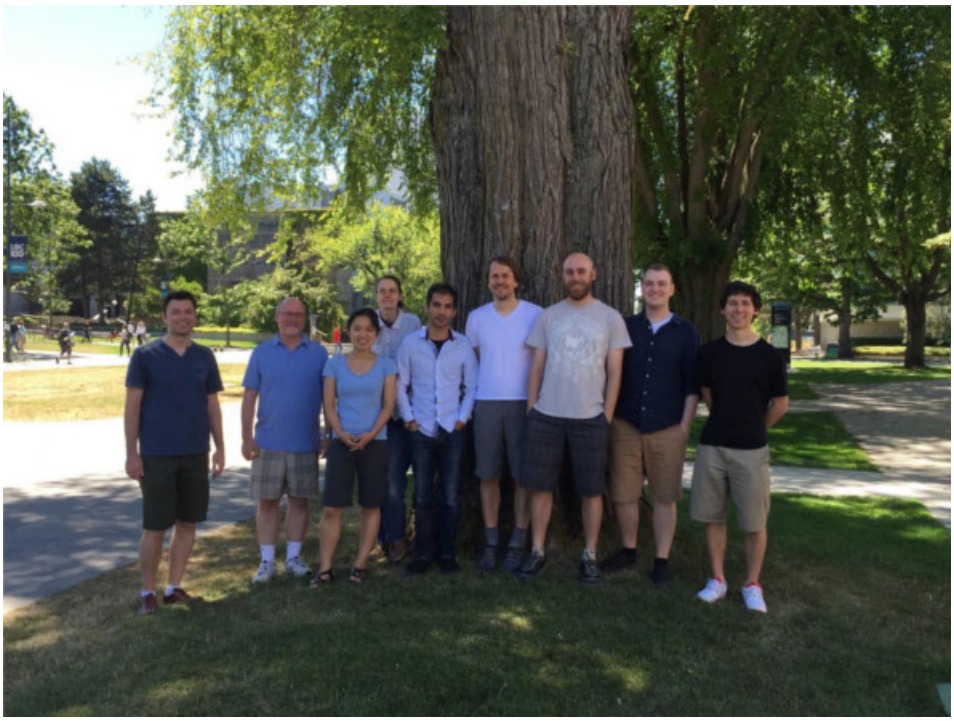

Bibliography

[1] D.M. Stamper-Kurn and J.H. Thywissen, arXiv:1111.6196 [cond-mat.quant-gas].

[2] Bakr, W.S., J.I. Gillen, A. Peng, S. Folling, and M. Greiner, *Nature* **462**, 74 (2009).

[3] T. Gericke, P. Wurtz, D. Reitz, T. Langen, and H. Ott, *Nature Physics*, **4**:949, (2008)

[4] Dare, K.M., B.Sc. thesis, University of British Columbia (2014).

[5] T. C. Li, H. Kelkar, D. Medellin, and M. G. Raizen, *Opt. Express* **16**, 5465 (2008).

Appendix A

Python Scripts

This appendix contains the Python scripts referenced in this report.

A.1 150713-fwhm4.py

This script will prompt the user for a pinhole image. It will output the FWHM of the pinhole image in pixels. The script will also generate a graph of the FWHM along the x-axis and y-axis of the image.

```
# 2015-07-13
# This program will prompt the user for an image, determine the FWHM of the
# pinhole image and plot the data for the x/y axes.

import numpy as np
import scipy.optimize as opt
import PIL
from PIL import ImageFilter
from pylab import *
from Tkinter import Tk
from tkFileDialog import askopenfilename

##############################
## Define Gaussian Function ##
##############################

def gauss(x, p): # p[0]==mean, p[1]==stdev
    return 1.0/(p[1]*np.sqrt(2*np.pi))*np.exp(-(x-p[0])**2/(2*p[1]**2))

#####################################
## Import Image; Find Brightest Spot ##
#####################################

Tk().withdraw() #keep the root window from appearing
```

```
filename = askopenfilename() #show an "Open" dialog box and return the path

im = PIL.Image.open(filename).convert("L")
imArr = np.array(im, dtype=float)

bg = np.average(imArr)
imArr = imArr - bg #this is needed to fix a bug in the Gaussian fitting

im2 = im.filter(ImageFilter.GaussianBlur(radius=2)) #filter image
imArr2 = np.array(im2, dtype=float)
coords = unravel_index(imArr2.argmax(), imArr2.shape) # get spot coords

i = 50 #specify the range of pixel values to consider around the bright spot

###################################
## Find & Plot FWHM for X/Y Axes ##
###################################

f = plt.figure(figsize=(18,5))

x = np.arange(coords[1] - i, coords[1] + i, dtype=np.float) #do x-axis first
y = imArr[coords[0], coords[1] - i:coords[1] + i]

p0 = [coords[1], coords[0]]

title = 'FWHM (x-axis)'

for j in range(1,3):

y /= ((max(x) - min(x)) / len(x)) * np.sum(y) #renormalize to a proper Gaussian

errfunc = lambda p, x, y: gauss(x, p) - y #distance to the target function
p1, success = opt.leastsq(errfunc, p0[:], args=(x, y))

fit_mu, fit_stdev = p1

FWHM = 2*np.sqrt(2*np.log(2))*fit_stdev
print title, FWHM
```

```
f.add_subplot(1,3,j)
plt.plot(x,y)
plt.plot(x, gauss(x,p1), lw=3, alpha=.5, color='r')
plt.axvspan(fit_mu-FWHM/2, fit_mu+FWHM/2, facecolor='g', alpha=0.5)
plt.xlabel('Pixel value', fontsize=13)
plt.title(title)
if j == 1:
plt.ylabel('Relative Pixel Intensity', fontsize=13) #only plot on y-axis

x = np.arange(coords[0] - i, coords[0] + i, dtype=np.float) #now do the y-axis
y = imArr[coords[0] - i:coords[0] + i, coords[1]]

title = 'FWHM (y-axis)'
j+=1

f.add_subplot(1,3,3)
plt.plot(coords[1], coords[0], 'b.', markersize=3)
plt.xlim(coords[1] - i/2, coords[1] + i/2)
plt.ylim(coords[0] - i/2, coords[0] + i/2)
plt.xlabel('Pixel x-value', fontsize=13)
plt.ylabel('Pixel y-value', fontsize=13)
plt.title('Approximate Centroid')
plt.imshow(im)

plt.show()

#FWHM implementation from:
#http://stackoverflow.com/questions/10582795
#/finding-the-full-width-half-maximum-of-a-peak

##################################
### WAYS TO IMPROVE THIS CODE ###
##################################

#fix the bug for when plotting the FWHM for the y values
#fit an Airy function instead of a Gaussian
#subtract an actual background image
```

A.2 150714-mag.py

This script determines the magnification of the imaging system when given two translated pinhole images.

```
# 2015-07-14
# This program will take two images of a pinhole and calculate the magnification
# based on the distance the pinhole was translated.

import numpy as np
import PIL
from PIL import ImageFilter
from pylab import *
from Tkinter import Tk
from tkFileDialog import askopenfilename

#######################################
## Import Image; Find Brightest Spot ##
#######################################

Tk().withdraw() #keep the root window from appearing
filename1 = askopenfilename() #show an "Open" dialog box and return the path
filename2 = askopenfilename()

im1 = PIL.Image.open(filename1).convert("L")
im1_filt = im1.filter(ImageFilter.GaussianBlur(radius=2)) #filter image
im2 = PIL.Image.open(filename2).convert("L")
im2_filt = im2.filter(ImageFilter.GaussianBlur(radius=2))

im1Arr = np.array(im1_filt, dtype=float)
im2Arr = np.array(im2_filt, dtype=float)

coords_im1 = unravel_index(im1Arr.argmax(), im1Arr.shape)
coords_im2 = unravel_index(im2Arr.argmax(), im2Arr.shape)

#################################
## Find Bright Spot Separation ##
#################################
```

```
dist = abs(coords_im1[1] - coords_im2[1]) * 3.75  #each pixel is 3.75 microns

########################
## Find Magnification ##
########################

translation = 50 #define translation dist of pinhole (50 microns here)

mag = dist/translation

print "The approximate magnification is", mag, "times."

f = plt.figure(figsize=(12,5))
f.add_subplot(1,2,1)
plt.plot(coords_im1[1], coords_im1[0], 'b.', markersize=3)
plt.imshow(im1)
f.add_subplot(1,2,2)
plt.plot(coords_im2[1], coords_im2[0], 'b.', markersize=3)
plt.imshow(im2)
plt.show()

################################
### WAYS TO IMPROVE THIS CODE ###
################################

#use a loop for the second image instead of doing everything twice
#prompt user for two image paths instead of having to edit the source code
#prompt user for the translation distance instead of having to edit the program
```

Appendix B

Apogee Alta U32 CCD Camera

When plugged into a computer via USB, the Apogee Alta U32 CCD Camera is not recognized. The fans turn on but the LED lights do not turn on (they did previously). The error message is

```
USB Device Not Recognized: One of the USB devices attached to this computer
has malfunctioned, and Windows does not recognize it.
```

Another error message that we received:

```
Code 43: Windows has stopped this device because it has reported problems.
```

I corresponded with Josh Calkins, a product support engineer at Andor Technology, regarding this problem. He stated that the problem we experienced sounds like a failure of the USB controller in the camera.

The camera, drivers and software were tested on a different computer without any luck. Multiple USB ports and USB cords were tried. Since the camera has serial ports, I asked if a work-around was possible using these ports. Calkins stated:

> Given that the USB connectivity doesn't work with another PC and the details of the error, I think that it's highly likely that the USB controller has failed. Unfortunately, the manufacturer of that controller discontinued it back in 2013 so we cannot repair it. The only way to get USB connectivity working again would be to upgrade the electronics to the current Alta F revision. This process would require you to send the camera to us for a few weeks.
>
> Regarding a workaround, the USB controller circuitry does not interact with the Ethernet ports, so you should be able to image with the camera via a local area network. The cable you'll need is a standard Cat5 Ethernet cable. I've attached a PDF of our camera installation guide. Details about connecting to the camera via a network start on page 10. Please note that while the instructions say they're for the Aspen line of camera, the steps are virtually identical for your camera (current Alta cameras only have USB, no Ethernet). Also, the camera does not have a preset IP address, so the router you connect it to must have DHCP to assign an IP address to the camera.
>
> The download times are slower over a network than via USB, but you should still be able to get back up and running.

Figure B.1: The Apogee Alta U32 camera.

He added:

> The label likely says Serial A and Serial B, but the physical port should be sized for a Cat5 cable. The Aspen electronics has the same port and protocols, the product management and labeling people just decided to change from 'Serial' to 'Ethernet' at some point.

We decided to test the power supply. Using a multimeter, the power supply itself was found to deliver the expected 12 V. We then attached the camera to a DC power supply at 12 V. We could only get up to 0.8 A of current at this voltage. The camera is supposed to operate at 40 W so we expected the current to go up to 3.3 A.

Regarding this result, Calkins responded:

> Regarding the power supply, the low current is to be expected. The current will only increase to the max 3.3 amps once the camera is connected to a PC and commanded to have the cooler turned on at max power.
>
> Regarding the serial port size mentioned in your other email, that is a new one to me. I checked the history of the serial number and found that the camera was manufactured in 2007, six years prior to Andor acquiring Apogee. I haven't been able to find any records about an electronics revision with an RJ12 port.
>
> If you're not successful in rigging up an RJ45 to RJ12 converter, I think that the only option left would be to have the camera sent to us for an upgrade to the latest electronics.

We then tried to rig up a RJ45 to RJ12 converter that could connect the serial port on the camera to an ethernet cord in the lab. Unfortunately, we were unsuccessful in rigging this up. It is highly likely that we made an error when setting it up and mixed up the wires. Unfortunately, we had to abandon troubleshooting the Apogee camera at this point because it was threatening to take up too much time. At the end of this project, the converter components were left in the lab with the camera.

Calkins sent me a document that has some information on the serial ports. This document is called AltaDevApi.pdf and can be found in the 'Michael's Documents' folder of the lab DropBox. Information regarding the serial ports starts on page 55.

Appendix C

CAD Drawings

The drawings presented in this appendix were created in SolidWorks. All parts were made out of aluminum and machined in the Department of Physics and Astronomy workshop in June 2015.

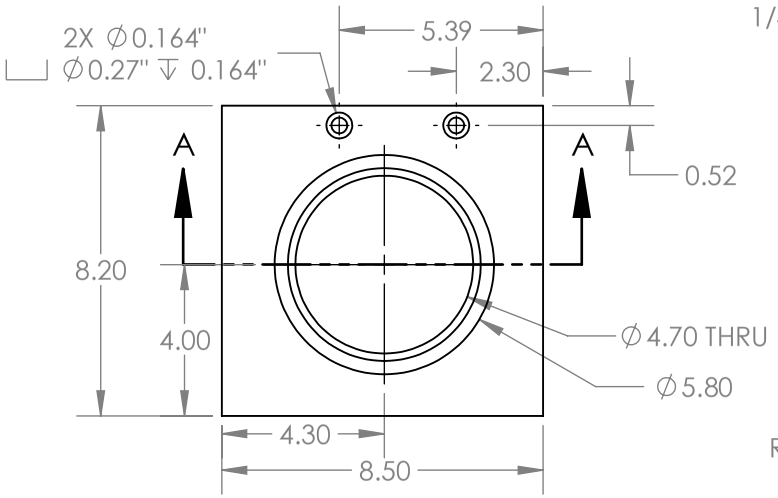

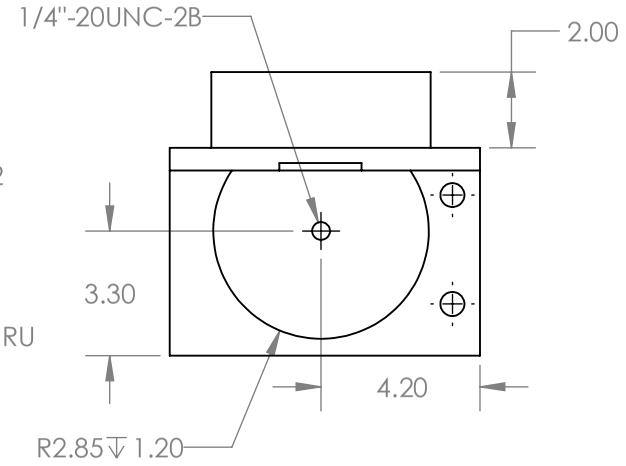

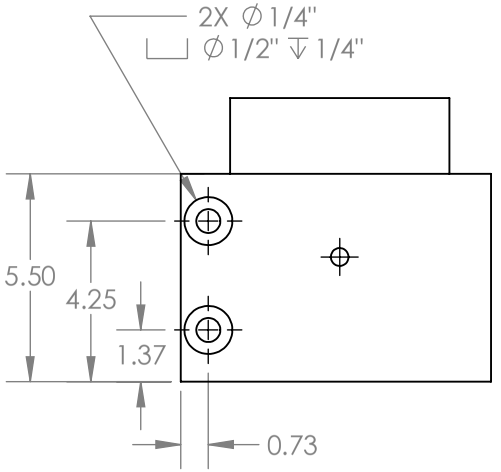

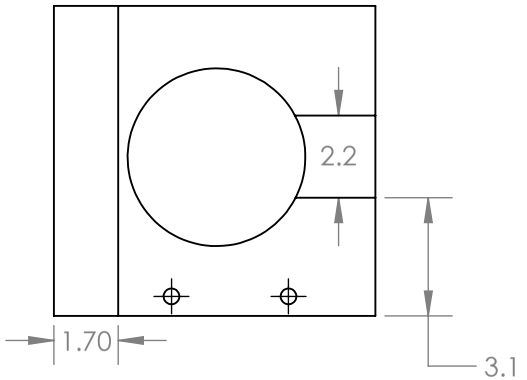

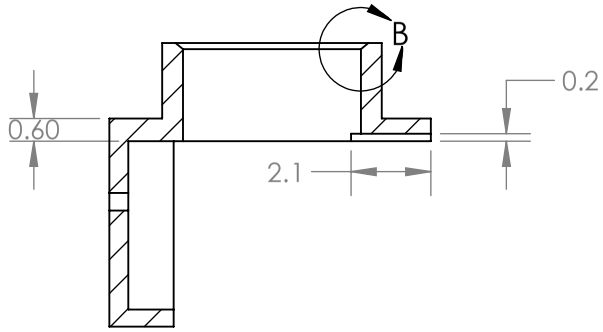

SECTION A-A

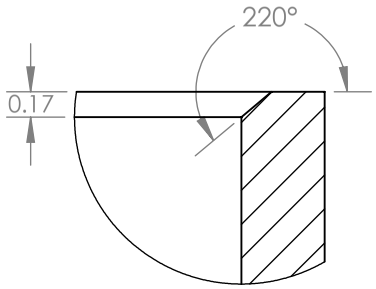

DETAIL B
SCALE 2 : 1

		UNLESS OTHERWISE SPECIFIED:		NAME	DATE
		DIMENSIONS ARE IN CM TOLERANCES: FRACTIONAL ± ANGULAR: MACH ± BEND ± TWO PLACE DECIMAL ± THREE PLACE DECIMAL ±	DRAWN	M KINACH	2015-05-22
			CHECKED		
			ENG APPR.		
			MFG APPR.		
		INTERPRET GEOMETRIC TOLERANCING PER:	Q.A.		
		MATERIAL	COMMENTS:		
NEXT ASSY	USED ON	FINISH			
APPLICATION		DO NOT SCALE DRAWING			

TITLE:

TOP

SIZE	DWG. NO.	REV
A		

SCALE: 1:2	WEIGHT:	SHEET 1 OF 1

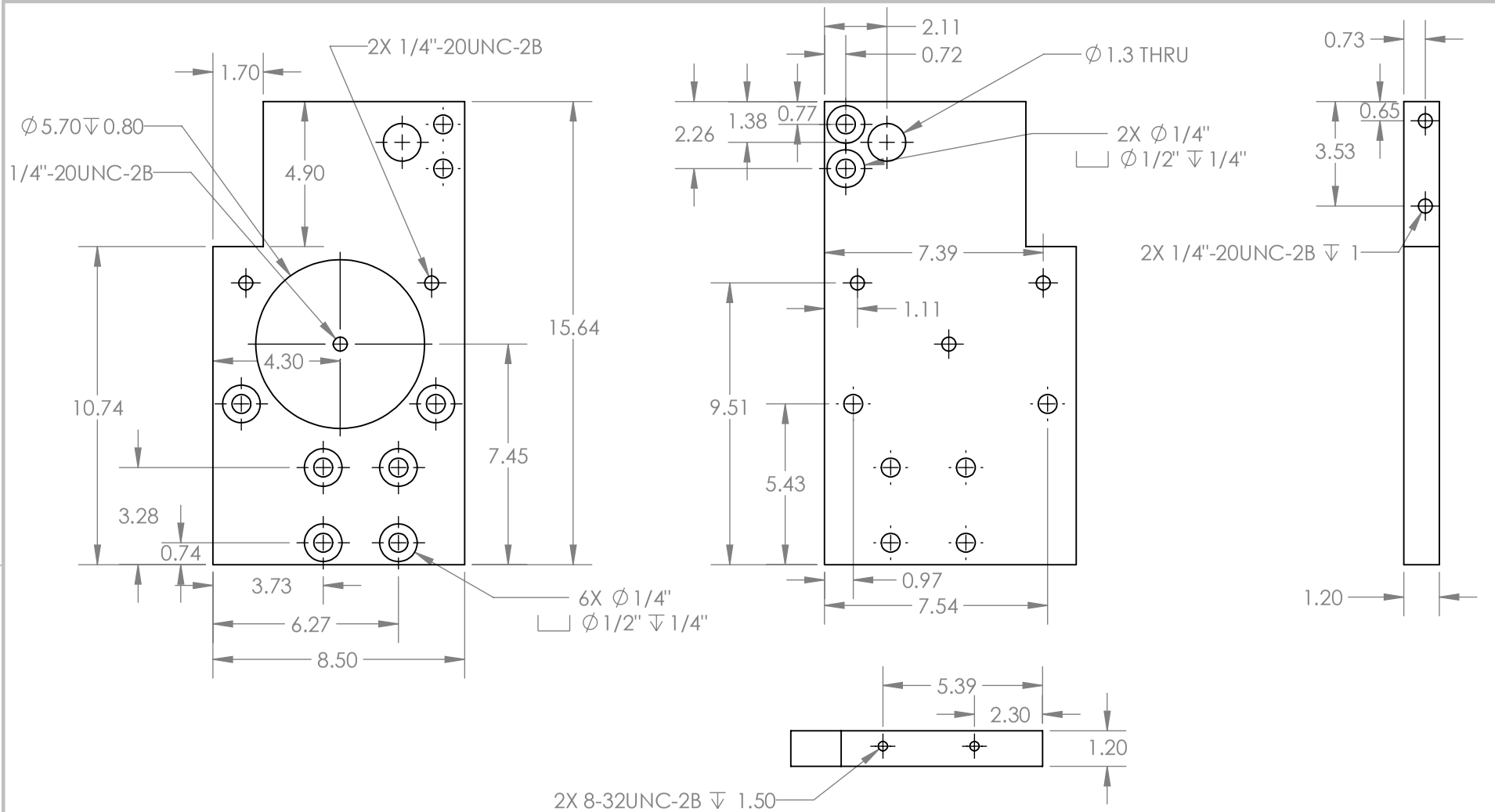

		UNLESS OTHERWISE SPECIFIED:		NAME	DATE
		DIMENSIONS ARE IN CM TOLERANCES: FRACTIONAL ± ANGULAR: MACH ± BEND ± TWO PLACE DECIMAL ± THREE PLACE DECIMAL ±	DRAWN		
			CHECKED		
			ENG APPR.		
			MFG APPR.		
		INTERPRET GEOMETRIC TOLERANCING PER:	Q.A.		
		MATERIAL	COMMENTS:		
NEXT ASSY	USED ON	FINISH			
APPLICATION		DO NOT SCALE DRAWING			

TITLE:

VERTICALv02

SIZE	DWG. NO.	REV
A		

SCALE: 1:2	WEIGHT:	SHEET 1 OF 1

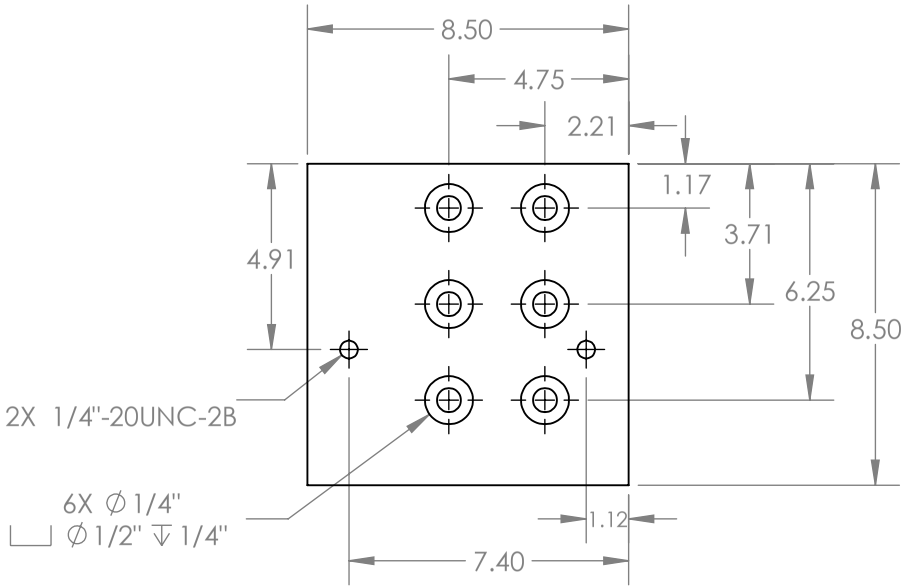

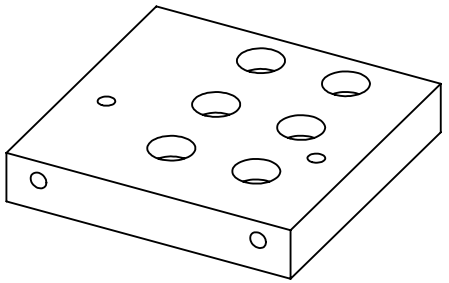

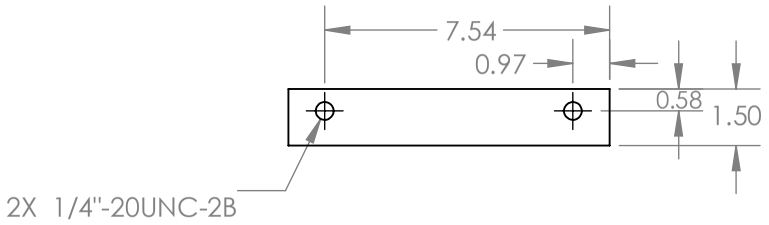

NEXT ASSY	USED ON	
APPLICATION		DO NOT SCALE DRAWING

UNLESS OTHERWISE SPECIFIED:

DIMENSIONS ARE IN CM
TOLERANCES:
FRACTIONAL ±
ANGULAR: MACH ± BEND ±
TWO PLACE DECIMAL ±
THREE PLACE DECIMAL ±

INTERPRET GEOMETRIC TOLERANCING PER:

MATERIAL

FINISH

	NAME	DATE
DRAWN	M.Kinach	2015-05-22
CHECKED		
ENG APPR.		
MFG APPR.		
Q.A.		

COMMENTS:

TITLE:

HORIZONTAL

SIZE	DWG. NO.	REV
A		

SCALE: 1:2	WEIGHT:	SHEET 1 OF 1

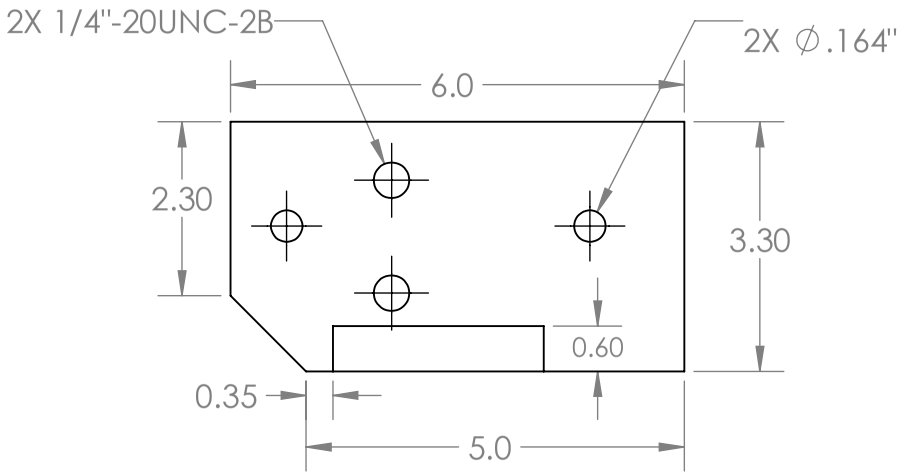

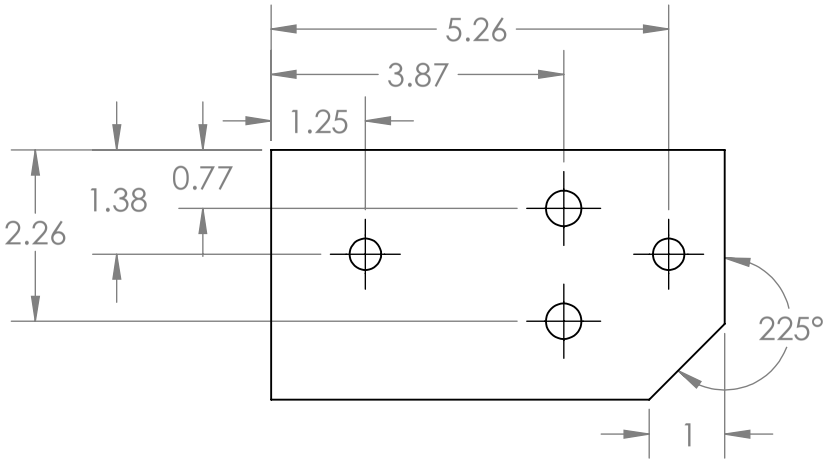

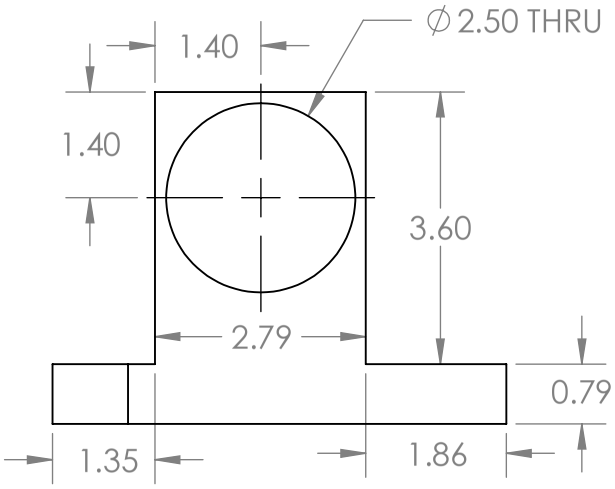

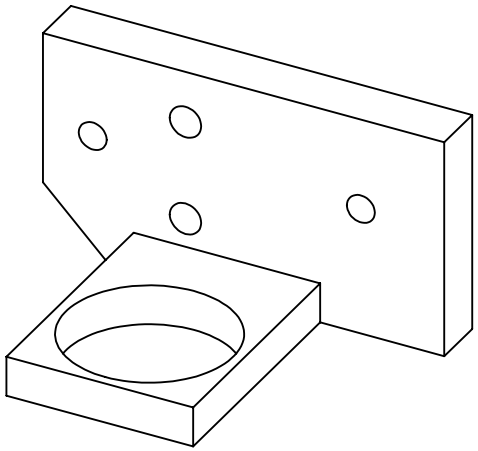

		UNLESS OTHERWISE SPECIFIED:		NAME	DATE
		DIMENSIONS ARE IN CM TOLERANCES: FRACTIONAL ± ANGULAR: MACH ± BEND ± TWO PLACE DECIMAL ± THREE PLACE DECIMAL ±	DRAWN	M Kinach	2015-05-22
			CHECKED		
			ENG APPR.		
			MFG APPR.		
		INTERPRET GEOMETRIC TOLERANCING PER:	Q.A.		
		MATERIAL	COMMENTS:		
NEXT ASSY	USED ON	FINISH			
APPLICATION		DO NOT SCALE DRAWING			

TITLE:

SIDEMOUNT

SIZE	DWG. NO.	REV
A		

SCALE: 1:1	WEIGHT:	SHEET 1 OF 1